NASA/TP-20260000432

Reliability Models and Demonstration of a Fault-Tolerant Motor Concept for Vertical Takeoff and Landing Vehicles

Timothy Krantz
Glenn Research Center, Cleveland, Ohio

James Swanke
H3X Technologies, Louisville, Colorado

Thomas Jahns
University of Wisconsin-Madison, Madison, Wisconsin

June 2026

NASA STI Program Report Series

Since its founding, NASA has been dedicated to the advancement of aeronautics and space science. The NASA scientific and technical information (STI) program plays a key part in helping NASA maintain this important role.

The NASA STI program operates under the auspices of the Agency Chief Information Officer. It collects, organizes, provides for archiving, and disseminates NASA's STI. The NASA STI program provides access to the NTRS Registered and its public interface, the NASA Technical Reports Server, thus providing one of the largest collections of aeronautical and space science STI in the world. Results are published in both non-NASA channels and by NASA in the NASA STI Report Series, which includes the following report types:

- TECHNICAL PUBLICATION.
  Reports of completed research or a major significant phase of research that present the results of NASA programs and include extensive data or theoretical analysis. Includes compilations of significant scientific and technical data and information deemed to be of continuing reference value. NASA counterpart of peer-reviewed formal professional papers but has less stringent limitations on manuscript length and extent of graphic presentations.

- TECHNICAL MEMORANDUM.
  Scientific and technical findings that are preliminary or of specialized interest, e.g., quick release reports, working papers, and bibliographies that contain minimal annotation. Does not contain extensive analysis.

- CONTRACTOR REPORT.
  Scientific and technical findings by NASA-sponsored contractors and grantees.

- CONFERENCE PUBLICATION.
  Collected papers from scientific and technical conferences, symposia, seminars, or other meetings sponsored or cosponsored by NASA.

- SPECIAL PUBLICATION.
  Scientific, technical, or historical information from NASA programs, projects, and missions, often concerned with subjects having substantial public interest.

- TECHNICAL TRANSLATION.
  English-language translations of foreign scientific and technical material pertinent to NASA's mission.

Specialized services also include organizing and publishing research results, distributing specialized research announcements and feeds, providing information desk and personal search support, and enabling data exchange services.

For more information about the NASA STI program, see the following:

- Access the NASA STI program home page at http://www.sti.nasa.gov

NASA/TP-20260000432

Reliability Models and Demonstration of a Fault-Tolerant Motor Concept for Vertical Takeoff and Landing Vehicles

Timothy Krantz
Glenn Research Center, Cleveland, Ohio

James Swanke
H3X Technologies, Louisville, Colorado

Thomas Jahns
University of Wisconsin-Madison, Madison, Wisconsin

National Aeronautics and
Space Administration

Glenn Research Center
Cleveland, Ohio 44135

June 2026

This work was sponsored by the Advanced Air Vehicles Program
at the NASA Glenn Research Center.

Level of Review: This material has been technically reviewed by expert reviewer(s).

This report is available in electronic form at https://www.sti.nasa.gov/ and https://ntrs.nasa.gov/

NASA STI Program/Mail Stop 050
NASA Langley Research Center
Hampton, VA 23681-2199

Contents

Reliability Models and Demonstration of a Fault-Tolerant Motor Concept for Vertical Takeoff and Landing Vehicles

Timothy Krantz
National Aeronautics and Space Administration
Glenn Research Center
Cleveland, Ohio 44135

James Swanke
H3X Technologies
Louisville, Colorado 80027

Thomas Jahns
University of Wisconsin-Madison
Madison, Wisconsin 53706

Summary

This report documents the completion of the Revolutionary Vertical Lift Technology Project Annual Performance Indicator 24-3.2.4.1: “Apply and document reliability prediction for high reliability motor concept.” Two modeling tools were completed for calculation of reliability of fault-tolerant (FT) motors, and key FT operations of a modular FT motor were demonstrated experimentally. The two models are complementary tools for the stakeholder and user community. Both models employ Markov chain theory. The first model is a time-homogeneous Markov chain model, and the second is a time-inhomogeneous Markov-Weibull model. This report’s main sections are as follows: 1.0 Introduction, 2.0 Theory, 3.0 Motor Reliability Models, 4.0 Validation of FT Operation by Hardware Demonstration, and 5.0 Concluding Remarks. Novel contributions to the field include development of a modular FT motor concept for electrified vertical takeoff and landing (eVTOL) application, solution methods to solve the reliability calculations, development of figures of merit, and the introduction of “linked chains” to formulate a building-block approach for time-inhomogeneous Markov-Weibull modeling of motor reliability. Example case studies have been completed, and results are provided and discussed herein. A four-module FT motor concept was developed to a preliminary-design level of detail. This eVTOL FT motor concept was designed for galvanic, magnetic, and thermal isolation of stator winding faults. The reliability of the concept motor was calculated using a time-inhomogeneous Markov chain model. Employing average failure rate as a metric, 570 times greater reliability was achieved as compared to a baseline motor without fault tolerance. A demonstrator motor was built and tested. The testing demonstrated the key features of FT operation and validated the essential premises of the FT motor concepts presented herein. The experiments included successful demonstration of the feasibility of the following four key FT features: (1) terminal open-circuit operation, (2) thermal isolation after fault, (3) terminal short-circuit operation, and (4) internal short-circuit operation. These works indicate that FT modular motor drives offer promise for addressing the daunting reliability gap that electric aircraft propulsor drives are facing relative to the best conventional motor drive technology that is available today.

1.0 Introduction

This report documents the description and hardware demonstration of a modular fault-tolerant (FT) motor concept for an electrified vertical takeoff and landing (eVTOL) concept vehicle. The report also documents the completion of two new analysis methods for calculating the reliability of FT motors. The two models are complementary tools for motor reliability prediction; the first is better suited to compare conceptual motor designs, whereas the second is better suited to predict reliability of a more detailed motor design. The accomplishments reported herein support the NASA Aeronautics Mission Directorate’s vision of a future state realizing extensive use of vertical lift vehicles for transportation and services, including new missions and markets (NASA 2023).

Darmstadt et al. (2019) identified failure modes and hazards associated with the propulsion systems of several emerging advanced air mobility vertical lift concept vehicles. They evaluated the propulsion system failure modes and effects and concluded that subsystem reliability must be improved to meet anticipated regulation requirements. The functional reliability of aircraft motor and motor drive subsystems can be improved via appropriate FT topology, a subject that is an active research topic. Wang et al. (2023) provided a state-of-the-art review of

FT motor technology for aircraft. The work herein provides a pair of tools to model and predict reliability of FT motor designs.

The motor reliability prediction methods will be described in detail in the following sections. The first modeling method was developed in collaboration with the University of Wisconsin. The university took the lead research role, and NASA provided guidance during monthly task review discussions. The mathematical approach of the first model required the assumption that motor components have constant hazard-of-failure rates. The work at the university also included hardware validation testing of a prototype FT motor to demonstrate the feasibility of FT features after a fault condition. All details of the first model and validation experiments have been openly published (Swanke, Zeng, and Jahns 2021; Swanke and Jahns 2022; Swanke 2023; Swanke et al. 2023; Jahns and Swanke 2024). This report includes some text, figures, and tables taken verbatim from the referenced reports.

The second model reported herein was developed to characterize the reliability of motors with increased fidelity. For this model, components of the motor have increasing hazards of failure with respect to time. This model was developed in-house by NASA Revolutionary Vertical Lift Technology (RVLT) Project researchers.

2.0 Theory

In Section 3.0, motor reliability models will be defined, discussed, and used to quantify the reliabilities of FT motor concepts for an eVTOL concept vehicle. In this section, the theory needed for these motor reliability models is introduced and discussed. The information to follow includes reliability concepts (Section 2.1), mathematics and notation (Section 2.2), probabilistic life models (Section 2.3), Markov chain theory and methods (Sections 2.4 and 2.5), and figures of merit (FOMs) used to compare and evaluate concepts (Section 2.6).

2.1 Reliability Concepts

2.1.1 Reliability

Reliability is often defined as “the probability that a system, vehicle, machine, device, and so on will perform its intended function under operating conditions for a specified period of time” (Meeker and Escobar 1998, 2). In this work, the “device” is an electric motor used to provide propulsive power. If the motor cannot deliver the demanded power to the propulsor, then the motor is considered failed. A failed motor condition does not necessarily imply a catastrophic flight event. A vehicle may be designed and operated in a manner to safely complete a mission even after one motor fails. However, for purposes of defining motor reliability in this report, a motor that cannot produce the demanded power (its intended function) is considered failed. The “operating conditions” are the flight conditions, including environmental conditions such as temperature, humidity, and so forth, and the “specified period of time” is the total operating time on the vehicle. Often, safety-critical devices of aircraft have a defined maximum allowed service time, and the device will be removed and replaced at the specified cumulative operating and/or calendar time.

2.1.2 Failure Time Distribution

The most widely used characterization of the reliability of a product is its failure time distribution (Meeker and Escobar 1998). Failure time distributions model stochastic processes and describe how populations of devices or systems fail over time. The values of the modeling parameters defining the distribution are usually not the primary interest of engineers or users of the devices or systems. Instead, engineers and users are interested in specific measures of the devices or systems, that is, the interest is in the characteristics of the failure time distributions. This work focuses on methods to determine two characteristics of particular interest, namely, the average failure rate and the mean time to failure (MTTF).

2.1.3 Average Failure Rate

The average failure rate is the average of the instantaneous failure rate over a specified time interval. For continuous-time reliability models, the average failure rate has units of inverse of time.

2.1.4 Mean Time to Failure

The mean time to failure is the expected life, that is, the first moment of the distribution of the failure times. It is a measure of the central tendency of the distribution. Mathematical definitions of MTTF and average failure rate will be provided in Section 2.2.

2.1.5 Fault Tolerance

Fault tolerance is the ability of a system or device to continue performing its intended function in the presence of faults (Johnson 1984). The fault-tolerance process for a motor can be divided into two main stages, the fail-safe stage and the FT operation stage (Wang et al. 2023). The first stage of fault tolerance is the fail-safe stage. When a fault occurs at this stage, the motor system can mitigate the fault in time to inhibit its spread to the healthy parts. In the FT operation stage, the motor system still has partial or full output capability after a fault and thus maintains the nominal and safe operation of the system.

2.1.6 Weibull Distribution

The Weibull distribution is a continuous-time probability distribution that is widely used to model failure times as well as other physical phenomena (Weibull 1939, 1951). From the theory of extreme values, one can show that the Weibull distribution models the minimum of many independent positive random variables from a certain class of distributions. This relationship to extreme value statistics provides a framework for studying the properties of the distribution and provides a theoretical basis for its application to failure data. A common justification for use of the Weibull distribution is empirical: it can model failure-time data regardless of whether the propensity to failure is increasing (appropriate for cumulative wear phenomena) or decreasing (appropriate for infant mortality phenomena), and the probability density function may be either skewed left or skewed right, depending on the value of the shape parameter that defines the distribution's essential characteristics.

2.2 Reliability Mathematics and Notation

This section provides mathematical definitions and notations for needed reliability concepts and failure time modeling. Nomenclature and symbols for this document are largely adopted from Meeker and Escobar (1998) and from the NIST/SEMATECH e-Handbook of Statistical Methods. Failure time of a motor is modeled herein as a continuous failure-time process. A useful concept for reliability of a motor (or motor component) is the failure-time distribution for failure time T'. The symbol T' denotes a nonnegative, continuous variable describing the failure time of a component, system, or population of units. Following here are several useful and interrelated mathematical functions of time for the distribution of failure time T'.

2.2.1 Cumulative Distribution Function

The cumulative distribution function (CDF) $F(t)$ gives the probability that a unit will fail before time t. $F(t)$ can also be interpreted as the proportion of units in the population that will fail before time t. Denoting probability as Pr, the equation defining the CDF is

$$F(t) = \Pr(T' \le t) \tag{1}$$

2.2.2 Probability Density Function

The probability density function (PDF) $f(t)$ represents the relative frequency of failure times as a function of time. The previously introduced CDF is the integral of the PDF from 0 to t, that is,

$$F(t) = \int_0^t f(x)\,\mathrm{d}x \tag{2}$$

$$f(t) = \frac{\mathrm{d}F(t)}{\mathrm{d}t} \tag{3}$$

2.2.3 Survival Function

The survival function $S(t)$ gives the probability of surviving beyond time t. The survival function is the complement of the CDF, that is,

$$S(t) = \Pr(T' > t) = 1 - F(t) \tag{4}$$

2.2.4 Hazard Function

The hazard function $h(t)$ expresses the propensity to fail in the next small increment of time. The hazard function is sometimes termed "hazard rate" or "instantaneous failure rate," among other names. The equation defining the hazard rate is

$$h(t) = \lim_{\Delta t \to 0} \frac{\Pr(t < T' \le t + \Delta t \mid T' > t)}{\Delta t} = \frac{f(t)}{S(t)} \tag{5}$$

and for small Δt,

$$h(t) \times \Delta t \approx \Pr(t < T' \le t + \Delta t \mid T' > t) \tag{6}$$

In the preceding expressions for $h(t)$, the terms inside the brackets for Pr express the conditional probability of failure of a unit given that the unit is known to have survived at time t.

2.2.5 Cumulative Hazard Function

The definition of cumulative hazard function $H(t)$ and its relationships to $F(t)$ and $S(t)$ are

$$H(t) = \int_0^t h(x)\,\mathrm{d}x \tag{7}$$

$$F(t) = 1 - \exp[-H(t)] \tag{8}$$

and therefore

$$H(t) = -\ln S(t) \tag{9}$$

2.2.6 Average Failure Rate

The average failure rate for the time interval from t_1 to t_2, $AFR(t_1,t_2)$, can be interpreted as a typical hazard rate value over the interval and can also be interpreted as the average fraction failing per unit time over the specified interval. The equation defining $AFR(t_1,t_2)$ is

$$AFR(t_1,t_2) = \frac{H(t_2) - H(t_1)}{t_2 - t_1} \tag{10}$$

For the special case of $t_1 = 0$, and applying Equation (9), one can determine $AFR(t)$ as

$$AFR(t) = \frac{-\ln S(t)}{t} \tag{11}$$

2.2.7 Mean Time to Failure

The mean time to failure, *MTTF*, is the expected time to failure after introduction to service. For a population of nonrepairable units where all units remain in service until failure, the *MTTF* of the population is defined as

$$MTTF = \int_0^\infty S(t)\mathrm{d}t \tag{12}$$

In some cases, units may have a defined retirement time, and units are removed from service at such retirement time even if no failure has occurred. The *MTTF* may then be defined as the total operating time divided by the total number of failures, and in general it is a function of time. For the special case in which the failure time distribution is an exponential distribution, the *MTTF* is a constant value for all operating times.

2.2.8 Weibull Distribution

The Weibull distribution is a continuous-time probability distribution and is widely used to model failure times. The Weibull distribution is one of a family of shape-scale-location distributions. The Weibull CDF to describe survivability can be defined as

$$S(t) = 1 - F(t) = \exp\left[-\left(\frac{t-\gamma}{\eta}\right)^\beta\right] \text{ for } t > \gamma \tag{13}$$

where S is probability of survival, F is probability of failure, t is the fatigue lifetime, β is the shape parameter, η is the scale parameter, and γ is the location parameter. Equation (13) is often called the three-parameter Weibull distribution. The scale parameter scales the mathematical function to engineering units. The location parameter translates the distribution function along the abscissa. The shape parameter defines the shape of the function. If the shape factor is equal to 1, then the hazard function is constant with time. Often, the location parameter is modeled and/or approximated as zero, and the distribution is then called the two-parameter Weibull distribution. A two-parameter Weibull distribution with a shape parameter equal to 1 is the exponential distribution.

2.3 Probabilistic Life Models

Reliability models of the lifetime of a component typically consist of (1) a life distribution model that represents the scatter of component life and (2) a stress-life model that represents the relationship between a nominal life and stress. Combining a life distribution model and a stress-life model establishes a probabilistic life model. The stress is the engineering parameter that influences the nominal life. The stress may be a load, voltage, temperature range of thermal cycling, velocity, strain, or other stressor depending on the device and failure mode. The nominal life is a specific characteristic of the life distribution—usually the mean, median, or a distribution percentile. Many such models appear in the literature. The motor reliability model described herein uses two models, the Power-Weibull model for bearings and the Arrhenius-Weibull model for motor windings.

2.3.1 Power-Weibull Model

The Power-Weibull model describes the influence of stress on lifetimes. The lifetimes are modeled as distributed Weibull (Nelson 1990). The relationship is based on the inverse power law, and therefore lesser stress produces longer lifetimes. Nelson comments that "the term 'law' suggests it is universally valid, which it is not. However, while usually not based on theory, the relationship is empirically adequate for many products" (Nelson 1990, 85). In this work, bearing life is modeled as Power-Weibull using the equation introduced by Palmgren (1959) that has been widely adopted in bearing design standards, that is,

$$L_{10} = \left(\frac{C}{P}\right)^p \tag{14}$$

where L_{10} denotes the lifetime of the tenth percentile of the probability distribution in millions of revolutions, C is the basic dynamic rating, P is the equivalent applied load, and p is the load-life exponent. The assumptions of the Power-Weibull model are as follows (Nelson 1990):

1. At any stress level V', the product life has a Weibull distribution.
2. The Weibull shape parameter β is a constant independent of V'.
3. The Weibull scale parameter η is an inverse power function of V'.

For the case of a three-parameter Weibull distribution, a fourth assumption is needed:

4. The ratio of the Weibull location γ parameter divided by the Weibull scale parameter η is a constant independent of V'.

2.3.2 Arrhenius-Weibull Model

The Arrhenius-Weibull model combines the Arrhenius life relationship and the Weibull distribution. The basis of the model is the Arrhenius rate law, where the rate of a chemical equation depends on temperature as follows:

$$rate = A' \exp\left[\frac{-E_a}{(kT)}\right] \tag{15}$$

where A' is a constant that is characteristic of the chemical reaction, E_a is the activation energy, k is Boltzmann's constant, and T is temperature on the absolute scale. The Arrhenius life model is based on the idea that failure occurs when some critical amount of the chemical has reacted, and thereby the lifetime is the ratio of the critical amount divided by the rate. Dakin (1948) applied the Arrhenius rate law to lifetime of electrical insulation, and this approach is now widely adopted in electrical insulation standards. The Arrhenius life equation relating the median lifetime to temperature is

$$L_{50} = A \exp\left(\frac{B}{T}\right) \tag{16}$$

where L_{50} denotes the median lifetime and A and B are constants that depend on geometry, size, fabrication methods, and other factors. The Arrhenius-Weibull model combines the Arrhenius life equation (Eq. (16)) with the Weibull distribution to define probability of failure after exposure to a constant temperature for a given exposure time. The assumptions of the Arrhenius-Weibull model are as follows (Nelson 1990):

1. At any temperature T, the product life has a Weibull distribution.
2. The Weibull shape parameter β is a constant independent of temperature T.
3. The natural log of the Weibull scale parameter η is a linear function of the inverse of absolute temperature T.

2.3.3 Linear Damage Model

The lifetime laws of Equations (14) and (16) apply when the operating load or experienced temperatures, respectively, are constant. When load or temperature varies, an additional model is required. A popular and commonly used approach is the linear damage model popularized by Miner (1945). Shimokawa and Tanaka (1980) introduced the following equation as a statistical version of Miner's rule:

$$\mathrm{E}\left(\sum_{i=1}^{m} \frac{n_i}{\overline{\overline{N_i}}}\right) = 1 \tag{17}$$

In Equation (17), E denotes the expected value of life, i = 1 to m are the m instances of temperatures T_i that were applied until failure, n_i is the duration of the application of temperature T_i, and $\overline{N_i}$ is the mean lifetime for a constant temperature T_i. Applying the same logic, for situations where failure has not yet occurred, a cumulative damage fraction D can be calculated as

$$D = \sum_{i=1}^{m} \frac{n_i}{\overline{\overline{N_i}}}, D < 1 \tag{18}$$

From damage fraction D, one can calculate the proportion of population failed by applying the Weibull equation presented in Equation (13). An assumption of the linear damage model is that the damage fraction is independent of the sequence of the varying temperatures. The linear damage law therefore has the Markov "memoryless" property.

2.4 Markov Chain Models

Markov (2004) introduced a model for stochastic processes. In this model, the outcome of a given experiment can affect the outcome of the next experiment. This type of process is called a Markov chain. Markov chain modeling is a state-space modeling method that can be applied for reliability assessment. The possible states of a system and the paths and probabilities for transition from one state to another are defined. Markov chains are popular for reliability modeling of systems that have more than two states (i.e., states beyond "fully healthy" and "failed"). Markov analysis is useful when dealing with medium-to-moderately sized systems. A practical upper limit of the system size is about 10 to 15 elements (Jackson 2013). Markov modeling calculates future states by analyzing probabilities of transitioning from a current state to the next. Markov chain models can be applied to FT and repairable systems as long as one accepts certain requirements from Markov theory. Meeker and Escobar (1998, 389) explain that "a Markov model is a special case of a state space model requiring (1) a memoryless property that future events depend only on the current state and not on the manner in which the system arrived at that state and (2) a stationary property that transition probability distributions do not change with time." Because of the requirement of the stationary property, to apply Markov chain models for reliability of systems, the failure time distributions of all components must be modeled as exponential functions, or equivalently as Weibull distribution functions having a Weibull shape parameter β = 1. A Markov chain model is typically created using state-space diagrams to visualize and keep track of the transition paths from one state to another. The resulting model comprises a set of differential equations describing the system. Mathematical theory, properties, and solution methods for Markov chains are elucidated by Rausand and Hoyland (2003). Darling and Norris (2008) explored and defined the conditions under which a Markov chain may be approximated by the solution to a differential equation, with quantifiable error probabilities. Under such appropriate approximation, a continuous-time Markov chain model can be concisely expressed in differential equation form, using matrix notation, as

$$\left(\dot{\boldsymbol{X}}\right) = \mathbf{T}\boldsymbol{X} \tag{19}$$

where $\boldsymbol{X}$ is a vector of all the system states, $\dot{\boldsymbol{X}}$ denotes derivative with respect to time t, and $\mathbf{T}$ is the Markov transition matrix. Each term of the matrix $\mathbf{T}$ has units of inverse of time, that is, each term is the rate of transition from one state to another state. Equation (19) has a solution of the form

$$\boldsymbol{X} = e^{\mathbf{T}t}\boldsymbol{X}_0 \tag{20}$$

Swanke and Jahns (2022) describe a process for determining analytical *MTTF* expressions from Equation (19) by employing Laplace transforms and the final value theorem. The *MTTF* expression is given by

$$\begin{aligned} MTTF &= \lim_{s\to 0}\left[s\cdot\mathcal{L}\left\{\int_0^t \left(\boldsymbol{H} + \sum \boldsymbol{M}\right)\mathrm{d}t\right\}\right] \\ &= \boldsymbol{H}(0) + \sum \boldsymbol{M}(0) \end{aligned} \tag{21}$$

where $\mathcal{L}$ denotes the Laplace transform to the s-domain, $\boldsymbol{H}$ denotes healthy states, and $\boldsymbol{M}$ denotes faulted states.

Continuous-time Markov chain models may also be expressed as finite difference equations. Such an approach is used extensively for decision-making in the medical field (Beck and Pauker 1983; Sonnenberg and Beck 1993). The finite difference equation form can be expressed as

$$\boldsymbol{X}_{i+1} = \mathbf{P}\boldsymbol{X}_i \tag{22}$$

where $\boldsymbol{X}$ transitions from discrete time instance i to discrete time instance $i+1$ according to the Markov matrix $\mathbf{P}$. Each term P_{jk} of square matrix $\mathbf{P}$ is a conditional probability of transition from one state to another or, for case $j = k$, the conditional probability to remain in the same state. Therefore, $0 \le P_{jk} \le 1$, and the sum of the terms of each column equals 1. One should note that Equation (22) is a matrix multiplication of a square matrix and a column vector to determine future state from current state, and each term P_{jk} represents the conditional probability of transitioning "from state k to state j." The terms are sometimes defined in the literature as conditional probabilities "from j to k," and the future state is then found by matrix multiplication of a row vector times the transition matrix; in such definitions, the sum of the terms of each row equals 1. In this work, the formulation of Equation (22) is used.

2.5 Time-Inhomogeneous Markov Chain Models

Some practitioners of Markov theory consider that the term "Markov chain" is applicable only for processes where the transition matrix is constant, per the originating work of Markov and following the description in Section 2.4 by Meeker and Escobar (1998). However, the Markov modeling approach has been extended for situations where the transition matrix is permitted to change with time, and the terms "time-inhomogeneous Markov chain" and "semi-Markov chain" have been adopted. In all cases, the structure of the Markov chain model is fixed, that is, the number of states, definitions of the states, and transition pathways are fixed. Markov chains where the values of the terms of the transition matrix are functions of a global time clock are termed "time-inhomogeneous models." If the values of the terms are functions of local time clocks, then the models are termed "semi-Markov models" (Boyd and Lau 1998). In this work, a motor reliability model is presented based on a time-inhomogeneous Markov chain. Note that "nonhomogeneous Markov chain" and "time-inhomogeneous Markov chain" are used interchangeably in the literature, and "time-inhomogeneous" is adopted herein.

Whereas some time-inhomogeneous Markov models can have analytical solutions via Lie algebra (House 2012), time-inhomogeneous Markov models usually require numerical solution methods. There are two numerical solution method groups, namely, Monte Carlo methods and cohort methods. Monte Carlo methods take the viewpoint of modeling a single member of a population per simulation. Time and associated state memberships progress by a series of simulation steps. At each step, the possible transitions from the current state are stochastic, and a Monte Carlo random number is used to determine the transition path of the individual. Each simulation of another individual of a population can have a different state membership history with time. Compiling and analyzing results on many such simulations allows researchers to study the behavior of a population. Another solution approach is the cohort method. In this method, the many subjects of a population are distributed to initial state memberships, and then for each step of the simulation, fractions of the population will transition to different states per the transition probabilities. Cohort models are typically formulated as finite difference equations. Iskandar (2018) addressed the theoretical foundation of the cohort approach and showed that from the typical finite difference cohort formulation one can recover the continuous-time model in the form of differential equations. Iskander related the cohort solution approach to the underlying Chapman-Kolmogorov master equation and thereby established a firm mathematical foundation for the cohort approach.

Beck and Pauker (1983) compared Monte Carlo and cohort solution methods for Markov modeling. They state that Monte Carlo simulations of Markov chains provide greater flexibility and information detail relative to the cohort solution approach. However, the Monte Carlo approach is computationally intensive. For typical medical decision-making modeling, Beck and Pauker recommend performing on the order of 10^4 Monte Carlo runs. For very high reliability modeling, such as is needed for eVTOL, Monte Carlo solution approaches would require very large numbers of runs, far exceeding 10^4, while using sophisticated algorithms for pseudo-random number generation. Cohort solutions require fewer computations. Given these considerations, a cohort method is adopted herein for time-inhomogeneous motor reliability modeling. Modeling details will be provided in later sections.

2.6 Fault Tolerance Figures of Merit (FT-FOMs)

FT motor drives can be accomplished using a variety of topologies, as illustrated in Figure 1, where all three concepts are capable of continued operation after fault of a component or subsystem. Smith and Flew (1986) discussed the pros and cons of motor redundancy approaches for space mission needs. Subject matter expertise is needed to down-select candidate designs during conceptual design processes. To supplement and guide subject matter expertise, FOMs can be devised to help evaluate the relative merits of competing designs toward achieving performance objectives.

Numerous candidate FOMs for FT motors and power electronics have been proposed and studied in the literature. For example, FOMs based on performance indices such as machine shear stress and winding current density are commonly used to evaluate the electromagnetic and thermal performance of electrical machines (Lipo 2017). For power electronics components, Baliga's FOMs are used to compare the capabilities of power semiconductor switch devices at high switching frequencies (Baliga 1989; Sung, Han, and Baliga 2017). For FT machine drives, performance/degradation FOMs have been proposed, including the silicon overrating cost factor and the fault power rating factor (Welchko et al. 2004).

This section proposes a set of FT-FOMs to better quantify and compare the achievable system reliability benefits of candidate motor drive topologies, including the impact of undesired performance penalties (e.g., component overrating), to expand and enhance the more specialized performance-oriented metrics defined by Welchko et al. (2004). The intent of these metrics is to provide users some new tools to perform high-level quantitative comparisons between candidate FT topologies that can be helpful for carrying out down-selection exercises. This section also provides a proposed procedure for calculating and applying these metrics using Markov chains, as well as a discussion on how to use the proposed metrics with FT machine drive topologies. Before introducing the definitions of these FT-FOMs, the following guidelines are provided to help inform potential users about some of the key characteristics of these metrics, the parameters that affect their magnitude and, finally, their engineering value and limitations:

1. The units of these FOM metrics vary widely and depend on their definitions. Whereas several are unitless because they are ratios of two parameters with the same units, others have unusual units, such as h/kg.
2. The quantitative values of the FOM metrics vary widely among the metrics, and any attempt to compare the quantitative values of two different FOM metrics is inappropriate. The appropriate approach is to compare the same FT-FOM metric for different candidate FT motor drive topologies.
3. The FOM metrics defined herein are such that higher values indicate better performers when comparing different candidate topologies for the same FT-FOM metric.
4. Each FOM metric is defined so that its value for a candidate topology depends on the ratio of the topology's mean time to failure (*MTTF*) to another performance metric, such as the *MTTF* of the motor drive modules, the frequency of repairs, the likelihood of single-point failures (SPFs), and so forth. The best topology for one of the FT-FOM metrics among a group of topologies that all share the same set of parameters might not be the best topology for a different FT-FOM.
5. The values of the FOM metrics depend on the parameter values (e.g., module failure rate, repair rate, and SPF rate) assigned for a candidate FT configuration. As a result, the ranking order of several candidate FT topologies evaluated for any selected FOM metric can change significantly as the values of these parameters are changed. The sensitivity of any chosen FOM metric to changes in any of the parameters, such as repair rate, can be conveniently investigated.

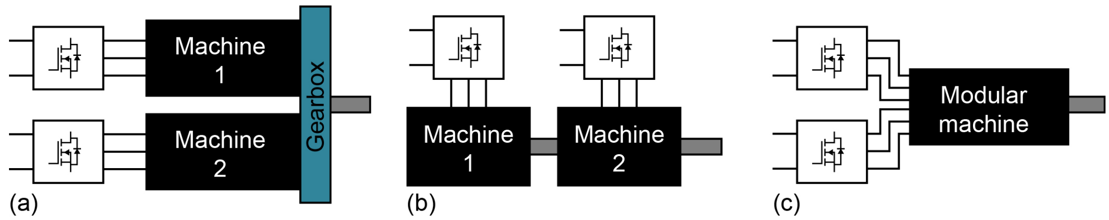

Figure 1.—Examples of FT machine drive topologies (Jahns and Swanke 2024). (a) Direct redundancy using two machines and shared gearbox. (b) Two stators on common shaft. (c) Modular machine drives.

The FT-FOMs proposed in the text to follow are functions of reliability and other performance metrics of interest. These FT-FOMs can be used to assess and compare candidate FT motor and drive concepts. The FOMs are presented in turn, using three groupings.

2.6.1 FOM Group 1: Focus on Average Reliabilities

This group of two FOMs was devised to help assess the reliability improvements by introduction of FT capability and are based on average values of life distributions. The two FOMs are

$$FTFOM_1 = \frac{MTTF}{MTTF_{std}} \quad [\text{unitless}] \tag{23}$$

and

$$FTFOM_2 = \frac{\Delta MTTF}{MTMF} \quad [\text{unitless}] \tag{24}$$

where

$$\Delta MTTF = MTTF - MTTF_{std} \quad [\text{h}] \tag{25}$$

and *MTMF* is the module group mean time to failure, that is, the first failure for a group of *n* identical FT modules introduced to create the FT capability. $MTTF_{std}$ is the *MTTF* of a system without FT operating capability.

2.6.2 FOM Group 2: Focus on Single-Point Failure and Repairability

This group of two FOMs was devised to help assess the impact of SPFs and repair rates of repairable components. The two FOMs are

$$FTFOM_3 = \frac{MTTF}{MTTSPF} \quad [\text{unitless}] \tag{26}$$

and

$$FTFOM_4 = \frac{MTTF_{HR}}{MTTF_{NR}} \quad [\text{unitless}] \tag{27}$$

where *MTTSPF* is the mean time to single-point failure and represents the expected time to failure for nonredundant components of the topology, $MTTF_{HR}$ is the mean time to failure for the topology using a high repair rate and $MTTF_{NR}$ is the mean time to failure with no repairs.

2.6.3 FOM Group 3: Focus on Reliability Relative to Performance Tradeoffs

This group of three FOMs was devised to help assess the tradeoff of improving reliability through the introduction of fault tolerance relative to other performance penalties, specifically added mass, steady-state power overrating, and maximum steady-state output power capability. These three FOMs are given in Equations (28) to (30).

$$FTFOM_5 = \frac{\Delta MTTF}{\Delta kg} \quad [\text{h/kg}] \tag{28}$$

$$FTFOM_6 = \frac{\Delta MTTF}{OF} \quad [\text{h}] \tag{29}$$

and

$$FTFOM_7 = \frac{\Delta MTTF}{KVAOF} \quad [\text{h}] \tag{30}$$

where Δkg is the increase of mass relative to the non-FT baseline, *OF* is the overrating factor needed such that a FT system can maintain rated power after a fault, and *KVAOF* is the kilovolt-amp overrating factor, which is the ratio of the sum total of total apparent power rating of all inverter modules divided by the apparent power rating of the inverter of the baseline design with no FT features.

2.6.4 FT-FOMs Summary

Swanke (2023) and Jahns and Swanke (2024) provide additional rationale and discussions of these FT-FOMs. The proposed FT-FOMs are summarized in Table I.

TABLE I.—SUMMARY OF PROPOSED FT-FOMS

Figure of merit grouping	FT-FOM	Calculation	Measure
Focus on average reliabilities	1	$\frac{MTTF}{MTTF_{std}}$	Measure of FT topology reliability normalized by MTTF of a baseline topology without FT
	2	$\frac{\Delta MTTF}{MTMF}$	Measure of topology reliability improvement normalized by MTTF of the module group (MTMF)
Focus on SPF and repairability	3	$\frac{MTTF}{MTTSPF}$	Measure indicating the dominance level of the SPF failure rate in determining FT topology reliability
	4	$\frac{MTTF_{HR}}{MTTF_{NR}}$	Measure of the influence level of the repair rate on the reliability of a FT drive topology
Focus on reliability improvement relative to another performance metric (i.e., tradeoffs)	5	$\frac{\Delta MTTF}{\Delta kg}$	Measure of FT drive topology reliability improvement gained per increment in topology mass
	6	$\frac{\Delta MTTF}{OF}$	Measure of FT drive topology reliability improvement relative to the level of required module overrating
	7	$\frac{\Delta MTTF}{KVAOF}$	Measure of FT drive topology reliability improvement relative to the combined steady-state kVA overrating of the inverter modules

3.0 Motor Reliability Models

In Section 2.0, Markov chain models and FT-FOMs were introduced and discussed. These engineering tools can be used together to evaluate candidate motor drive concepts, including those with FT topologies. In this section, two Markov chain reliability models are proposed and applied. A time-homogeneous model is discussed in Section 3.1, and a time-inhomogeneous model is discussed in Section 3.2.

3.1 Time-Homogeneous Markov Chain Modeling of Motor Drive Units for eVTOL

In this section, a time-homogeneous Markov-chain-based motor drive reliability modeling method is proposed and then applied. Per Markov chain theory, the transition probabilities are constants, and therefore this model assumes constant hazard and repair rates. First, a method to determine analytical solutions for the *MTTF* of a Markov chain is described by way of an example having three states. Second, recommended procedures to determine *MTTF* for more complex Markov models are proposed and summarized. Third, a case study is completed to evaluate five candidate FT motor drive concepts, FOMs are determined, and results are compared to the baseline concept that is not FT.

3.1.1 Analytical Solution of Markov Chain for Determination of *MTTF*

In some instances, it may be desirable to produce analytical *MTTF* formulas for a given FT system to better understand the relationship between the underlying failure transitions and component failure rates. This process is illustrated using the elementary FT system-state diagram in Figure 2 of a modular topology approach to motor fault tolerance. In this example, there are three states, one each of a healthy state, a faulted state, and a failed state. This example includes a transition path that bypasses the faulted state, a SPF transition path.

In the example Markov model shown in Figure 2, the system will be in the failed state if any two modules become faulted or if a nonmodular component fails. The system may transition from the faulted state to the healthy state by a repair action. The Markov model comprises a set of three differential equations:

$$\begin{aligned} \dot{H} &= u \cdot M_1 - \left(\lambda_{m0} + \lambda_{s0}\right) \cdot H \\ \dot{M}_1 &= \lambda_{m0} \cdot H - \left(\mu + \lambda_{m1}\right) \cdot M_1 \\ \dot{FS} &= \lambda_{s0} \cdot H + \lambda_{m1} \cdot M_1 \end{aligned} \tag{31}$$

This example model has four transition rates: (1) λ_{m0}, the module fault rate from the healthy state, (2) λ_{m1}, the additional module fault rate, (3) λ_{s0}, the SPF rate, and (4) μ, the repair rate from the faulted state. The *MTTF* can be found by application of the Laplace transform method (Eq. (21)), and the solution is

$$MTTF = \frac{\lambda_{m0} + \lambda_{m1} + \mu}{\lambda_{m0} \cdot \lambda_{m1} + \lambda_{s0} \cdot \mu + \lambda_{s0} \cdot \lambda_{m1}} \tag{32}$$

From Equation (32), the module fault rates and the repair rate sum together to form the numerator, and the denominator is a sum of pairs of products of the transition rates. The SPF rate appears only in the denominator, and therefore a large SPF rate would result in an undesirable small value for *MTTF*. However, the SPF rate effect can be offset by a combination of small module fault rates combined with a rapid repair rate.

More complex models can be solved by the same procedure; further guidance is provided in Swanke (2023). Note that the number of differential equations will be equal to the number of states. The complexity of the *MTTF* analytical formula increases rapidly in these more complicated cases, but solutions can be found with the aid of symbolic math software tools.

3.1.2 Procedure for Evaluation of FT-FOMs

Swanke (2023) recommends a four-step procedure for evaluating FT-FOMs. The recommended procedure is summarized in Figure 3, and the following text provides some procedural guidance.

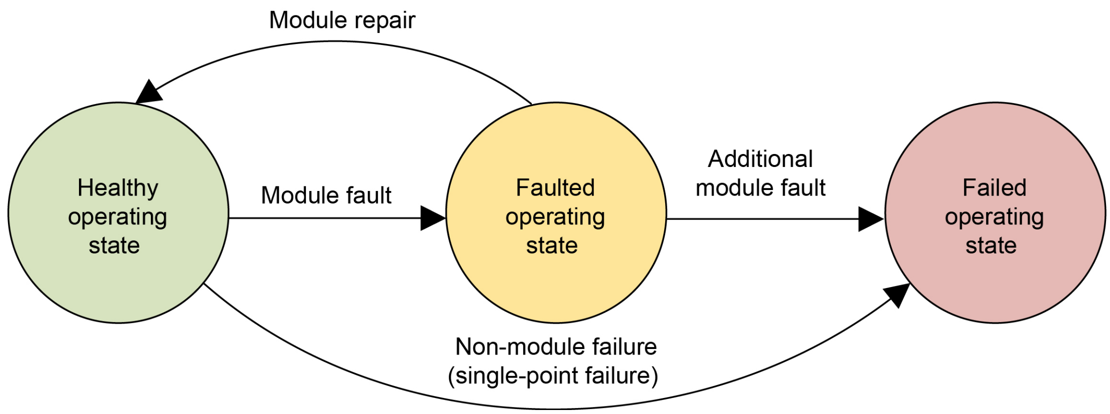

Figure 2.—Operating states (healthy, faulted, and failed) of a FT system and corresponding transitions (Jahns and Swanke 2024).

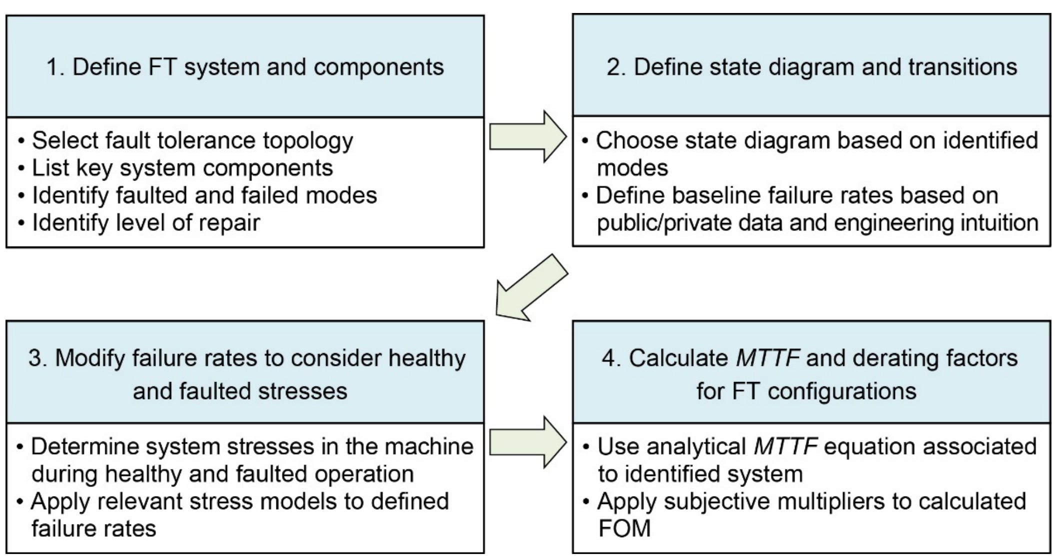

Figure 3.—Recommended procedure for evaluation of FT-FOMs for candidate FT systems (Jahns and Swanke 2024).

3.1.2.1 Step 1: Define FT Systems and Components

The first step is the definition of the FT system and its components. More specifically, this process involves identifying all relevant components in the FT system (switches, capacitors, machine windings, etc.), the associated fault modes and their interactions, the impact of repairing any faults, and the ultimate system failure mode. In addition, the user must define the desired system operating capabilities during each of the fault and failure modes.

3.1.2.2 Step 2: Define State Diagram and Transitions

The next step in the procedure is to organize the fault and failure modes identified in step 1 into healthy, faulted, and failed states based on their effects, leading to the development of a state diagram. In FT systems, simplifications are typically made when modeling a single module such that any component failure inside the module results in the same fault state, which typically is inoperability of the module. If there are n identical modules in the system with the same fault state, the fault modes for these n modules can be grouped together into a single equivalent fault state with a combined module failure rate that is n times that of a single module. Transitions between states are initiated by component failures and other failure events (e.g., damage from foreign objects), each of which is quantified by its associated failure rate. In many cases, the fault states are associated with several different component failures and other failure events. When this is the case, the overall fault transition probability is determined by forming the sum of the failure rates. Typical values of component failure rate can be obtained from user internal sources, component data sheets, or the published literature. Sample data for the modular machine study can be found in Swanke (2023). A FT system-state diagram will almost always have two additional important transition paths, namely, the SPF path quantified by λ_{s0}, and the repair transition path quantified by μ. The effects of these variables are discussed in detail by Swanke (2023). The state-space diagram should include all possible states and transition pathways. The states must be mutually exclusive, that is, at any instance of time, a member of the population has membership in one, and only one, state.

3.1.2.3 Step 3: Modify Failure Rates To Consider Operating Stresses

The failure transition values of step 2 can be modified to reflect expected operating stresses during both healthy and faulted operation. In many cases, it may be challenging to make significant modifications if this procedure is being used early in a FT topology screening process and specific design details of the studied FT topologies are unknown. However, parametric studies exploring the impact of postfault stress on FT system reliability are still possible and valuable in some cases. Some basic pre- and postfault stress details can be determined by understanding the FT topology itself and how the system reconfigures itself after a failure. In this procedure, the operating stress factors will be selected based on the concept of pi-factors suggested in MIL-HDBK-217F (1991), where a baseline component failure rate λ_{BL} is modified by multisource stress factors π_i, leading to an overall stressed failure rate. In general, it is recommended that users apply physical principles underlying component life-calculation formulas or make use of available datasheets of module components. Using this approach, the pi-factors can be extracted by ratioing life-estimation results.

3.1.2.4 Step 4: Calculate *MTTF* and Derating Factors for FT Configurations

A fully assembled Markov chain state diagram and associated equations of the studied candidate FT systems with numerical failure transitions can be assembled into matrix form, and *MTTF* can be found following from Equation (21). To calculate the FOMs of Table I requires some additional information.

To calculate $FTFOM_5$, one must estimate the added mass Δkg required to create a FT design relative to the mass of the baseline design without fault tolerance. It may be impractical at an early design stage to determine the extra mass with precision. However, it may be possible and sufficiently precise to estimate the mass of a candidate FT topology using available reference designs and then applying scaling factors as needed. When using the mass scaling factor approach, it is recommended to estimate the added mass for the power electronics and the motor by separate scaling factors. Such an approach results in an equation for added mass as

$$\Delta kg = (MMF - 1) \times m_{em} + (DMF - 1) \times m_{pe} \qquad (33)$$

where *MMF* is the machine-mass scaling factor, m_{em} is the mass of the baseline motor, *DMF* is the power electronics drive-mass scaling factor, and m_{pe} is the mass of the baseline power electronics. Jahns and Swanke (2024) provide additional guidance for selecting *MMF* and *DMF*.

To calculate $FTFOM_6$ and $FTFOM_7$, the overrating factors *OF* and *KVAOF* must also be selected, and values should be consistent with the particular FT topology. Finally, the FT-FOMs of Table I can be calculated. The results can be gathered and organized for evaluation to guide and inspire design selections, research investment strategies, configuration innovation, and so on.

3.1.3 FT Motor Drive Reliability: Time-Homogeneous Markov Chain Case Study

The purpose of the previously discussed case study was to illustrate and exercise the time-homogeneous Markov chain method for motor reliability. In this case study, six proposed designs were evaluated, one a baseline design with no FT features and five FT designs. The reliability assessment followed the procure depicted in Figure 3. Descriptions of the designs, stress factors, repair rates, derating factors, and mass multipliers that are needed to produce quantified results are given here, followed by presentation and discussion of results.

3.1.3.1 Design Descriptions

In this case study, six designs were studied, and the relative reliabilities were compared by assessing FT-FOMs. The six designs of the study are (1) baseline design without fault tolerance, (2) five-phase machine drive with two allowable switch failures, (3) a direct redundant motor drive, (4) a two-module motor drive (X2-MMD), (5) a four-module motor drive (X4-MMD), and (6) a four-module MMD with a redundant resolver, a redundant cooling system, and reduced-bearing SPF rates via a health monitoring system (X4-MMD+).

The baseline system design topology includes a two-level voltage source inverter (VSI). Components of this design include six metal-oxide-semiconductor field-effect transistor (MOSFET) devices with anti-parallel diodes, a single dc-link capacitor, and a three-phase machine winding set. Other components include a bearing pair, a coolant system, three current sensors, six gate drivers, a controller, and a rotor angular position resolver. Other components (rotor structure, magnets, etc.) are assumed to have much lower failure rates as compared to the failure rates of the preceding identified components and are ignored in this evaluation.

The five-phase machine drive VSI enables drive reconfiguration by adding phase legs to the baseline concept that provide phase redundancy for open-circuit faults, as shown in Figure 4. In the event of a switch or winding open-circuit fault, the faulted phase leg is isolated by opening the corresponding complementary switch. The remaining healthy phases are then able to continue operating, perhaps with some phase angle changes in their excitation, to retain a large fraction of the healthy drive's original output power capability. In this study, the five-phase VSI assumes that two open-circuit phase-leg faults can be tolerated before a failure.

The direct redundant motor drive is the simplest FT topology, applying redundancy directly to the baseline three-phase motor drive system. Two redundant motor drives are coupled together mechanically using a gearbox (Figure 5). In the event of a motor drive failure, the failed unit is decoupled from the gearbox and operation continues using the remaining healthy motor drive. It is also assumed that each of the two drives in the two-module topology is excited using a DC link voltage that is 50% of the value used for the baseline topology, lowering the voltage rating of all the inverter switches while their current rating is unchanged. If one of the two modules fails, the remaining healthy module must deliver approximately twice the current it supplies during normal healthy operation to return the topology to its full power capability. This increases the electrical and thermal stress on the healthy power switches that must be reflected in the stress factors for the inverter switches.

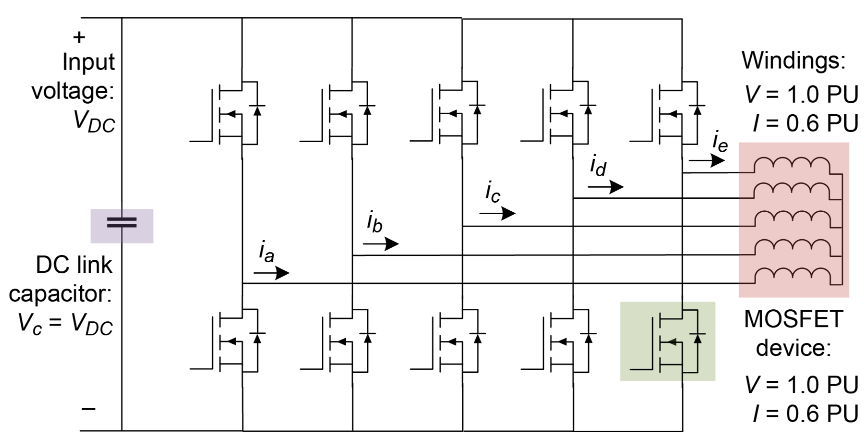

Figure 4.—Schematic representation of five-phase design with healthy component ratings noted (Jahns and Swanke 2024).

The three modular motor designs (X2-MMD, X4-MMD and X4-MMD+) implement redundancy at the power electronics and machine windings level. This is accomplished by dividing the single stator assembly into multiple three-phase winding sets, each supplied by its own independent power electronics. Discussion of machine control, galvanic isolation, thermal isolation, magnetic isolation, and experimental demonstration of fault tolerance of the modular machine concept can be found in Swanke, Zeng, and Jahns (2021) and Jahns and Swanke (2024). The X2-MMD variant has two modules; each delivers half of the rated power during healthy operation, like the direct redundant topology. Each module is assumed to operate with $V_{DC}/2$ and the same rated current as the baseline VSI topology ($V_{DC}/4$ for the four-module case). The two-module X2-MMD configuration is only capable of continuing operation following a single module fault, whereas the X4-MMD and X4-MMD+ designs are capable of continued operation following two module faults. The X4-MMD+ design is nearly identical to the X4-MMD except the total SPF rate is significantly reduced by adding modular redundancy for the resolver and the cooling system, thereby removing them from the SPF path. Only the bearings remain as single-point fault modes, and the transition to the failed state is reduced using a health and monitoring approach (see Jahns and Swanke (2024) for more details). Figure 6 is a schematic representation of the four quadrant X4-MMD concept.

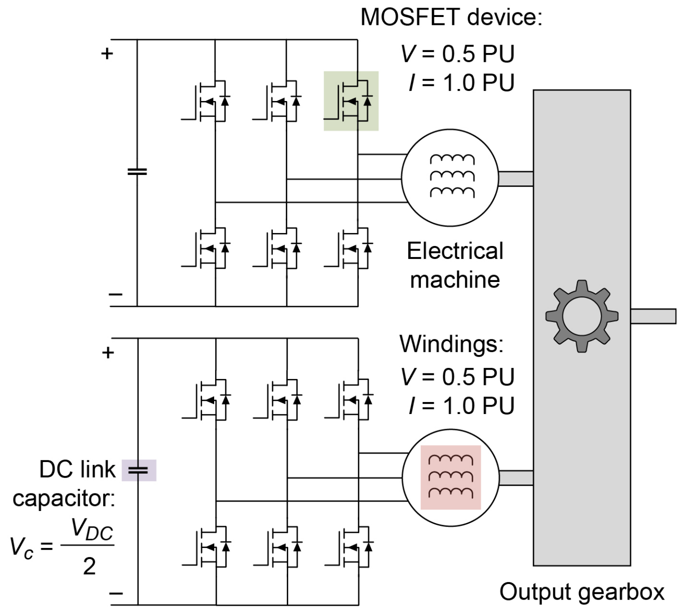

Figure 5.—Schematic representation of direct redundant drive design with healthy component ratings noted (Jahns and Swanke 2024).

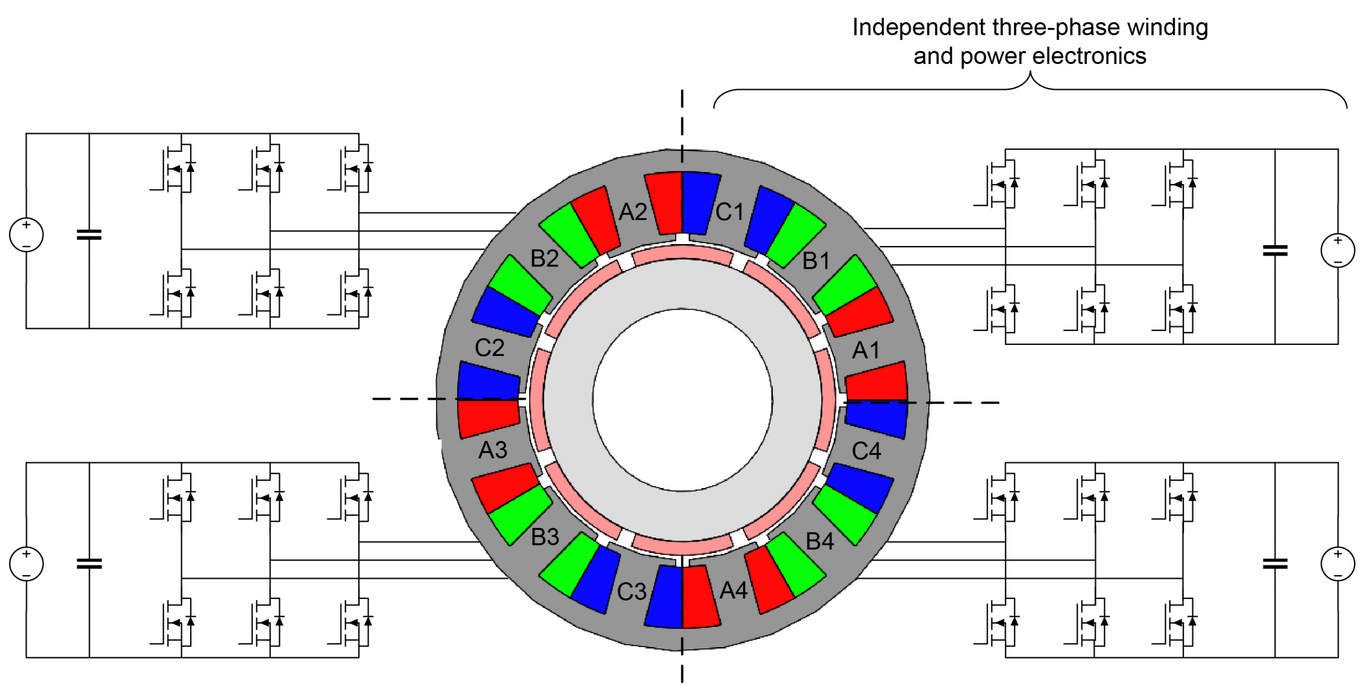

Figure 6.—Schematic representation of four-quadrant modular motor concept (Jahns and Swanke 2024).

A single DC input supply value is assumed for all of the candidate FT topologies. For topologies with multiple DC inputs, it is assumed these inputs are connected in series. In the event of a module fault, it is assumed the faulted module is bypassed by a short circuit across its DC input terminals, resulting in the total supply voltage being applied to the remaining series-connected healthy modules. A summary of the studied FT topologies and fault coverage capability for each of the five studied topologies is provided in Table II.

3.1.3.2 Baseline Failure Rates and Stress Factors

Baseline failure rates for evaluating the *MTTF* values of the shared FT topologies are summarized in Jahns and Swanke (2024). For the direct redundant configuration, the failure rate of the gearbox, one of the major SPF sources in this topology, is assumed to be equal to the bearing failure rate. The same component failure rates are applied to each topology in its healthy state to provide meaningful comparisons of the reliability characteristics for these topologies. However, the topologies operate with varying levels of postfault stress that are quantified using multiplicative stress factors. The determined and applied stress factors for this case study are summarized in Table III, with corresponding justifications addressed briefly in the following paragraphs.

Postfault stresses are heightened in all topologies because they are assumed to deliver full power output after a fault for this case study. The postfault healthy module phase current must increase in proportion to the machine overrating factor OF (see Swanke 2023), and the corresponding winding losses scale as OF^2. For purposes of this analysis, it is assumed that the machine and power electronics thermal system experience postfault temperature rises proportional to OF^2. Similar simplifications are made to consider the impact of unbalanced magnetic pull (UMP) on the rotor after the loss of a module (i.e., increased dynamic load on the bearing), which worsens as the number of faulted modules increases. For this analysis, it is assumed that the increase in bearing dynamic load ratio is proportional to the machine overrating factor OF. In some instances, the loss of subsequent phases or modules could reduce or completely cancel the unbalanced pull on the rotor (e.g., opposite modules). However, the possibility of unbalanced force cancellation will be ignored during this case study.

The direct redundant and modular configurations are defined to be connected in series resulting in higher module voltages after a fault. Machine winding voltage stress factors are estimated using the insulation lifetime relationships. Capacitor and device voltage stresses are assumed to use relationships presented in component datasheets. Voltage ratings of healthy device and winding insulation are assumed to be overrated to 200% of the component nominal operating voltages to allow for more reasonable voltage stress ratio values.

TABLE II.—STUDIED FT TOPOLOGIES AND FAULT COVERAGE CAPABILITY

Topology	Power electronics failure protection, X-yes, O-no			Machine failure protection, X-yes, O-no			Non-power electronics or machine failure protections and vulnerabilities	
	Switch short circuit	Switch open circuit	Capacitor	Terminal phase open	Terminal phase short	Internal short	Redundant components	SPFs
Baseline (two-level VSI)	O	O	O	O	O	O	-------------------------	Controller, resolver, current sensors, bearings, cooling system
Five-phase VSI	O	X	O	X	O	O	-------------------------	Controller, resolver, current sensors, bearings, cooling system
Direct redundancy	X	X	X	X	X	X	Controller, resolver, current sensors, bearings	Gearbox, cooling system
Two-module independent MMD	X	X	X	X	X	X	Controller, current sensors	Resolver, bearings, cooling system
Four-module independent MMD	X	X	X	X	X	X	Controller, current sensors	Resolver, bearings, cooling system
Four-module independent MMD with reduced SPF	X	X	X	X	X	X	Controller, current sensors, resolver, cooling system	Bearings

TABLE III.—DEVELOPED STRESS FACTORS FOR CASE STUDY

Topology	Component	Postfault stressor (π-factor)	π-factor, quantity	Notes
Five-phase design	Winding (M_1 state)	Temperature ($\pi_{cls,T,1}$)	3.0	Stresses related to first faulted state (M_1)
	Device (M_1 state)	Temperature ($\pi_{sw,T,1}$)	2.5	
	Winding (M_2 state)	Temperature ($\pi_{cls,T,2}$)	6.7	Stresses related to second faulted state (M_2)
	Device (M_2 state)	Temperature ($\pi_{sw,T,2}$)	5.1	
Direct redundant	Winding	Temperature ($\pi_{cls,T}$)	16.0	
	Winding	Voltage ($\pi_{cls,V}$)	32.0	
	Capacitor	Voltage ($\pi_{cap,V}$)	41.3	
	Device	Temperature ($\pi_{sw,T}$)	10.4	
	Device	Voltage ($\pi_{sw,\mathrm{V}}$)	403.0	
Two-module MMD	Winding	Temperature ($\pi_{cls,T}$)	16.0	
	Winding	Voltage ($\pi_{cls,V}$)	32.0	
	Capacitor	Voltage ($\pi_{cap,V}$)	41.3	
	Device	Temperature ($\pi_{sw,T}$)	10.4	
	Device	Voltage ($\pi_{sw,V}$)	403.0	
	Bearing	UMP (π_{brg})	8.0	
Four-module MMD	Winding (M_1 state)	Temperature ($\pi_{cls,T,1}$)	3.4	Stresses related to first faulted state (M_1)
	Winding (M_1 state)	Voltage ($\pi_{cls,V,1}$)	3.2	
	Capacitor (M_1 state)	Voltage ($\pi_{cap,V,1}$)	3.5	
	Device (M_1 state)	Temperature ($\pi_{sw,T,1}$)	2.8	
	Device (M_1 state)	Voltage ($\pi_{sw,V,1}$)	7.4	
	Bearing (M_1 state)	UMP ($\pi_{brg,1}$)	2.4	
	Winding (M_2 state)	Temperature ($\pi_{cls,T,2}$)	16.0	Stresses related to second faulted state (M_2)
	Winding (M_2 state)	Voltage ($\pi_{cls,V,2}$)	32.0	
	Capacitor (M_2 state)	Voltage ($\pi_{cap,V,2}$)	41.3	
	Device (M_2 state)	Temperature ($\pi_{sw,T,2}$)	10.4	
	Device (M_2 state)	Voltage ($\pi_{sw,V,2}$)	403.0	
	Bearing (M_2 state)	UMP ($\pi_{brg,2}$)	8.0	

3.1.3.3 Repair Rates

For all the *MTTF* and FT-FOM calculations, it is assumed that machine failures will be repaired within 24 operating hours on average, corresponding to a constant repair rate of μ = 1/24 or 0.0417 h^{-1}. The constant repair rate is assumed because a constant rate is needed for the time-homogeneous Markov chain approach. It is assumed that the system retains its ability to deliver its rated steady-state power until the system failure event occurs. The alternative of allowing for partial degradation of the system steady-state power delivery following a module fault is not considered here to avoid the additional computational complications such an approach would introduce. The calculation of $FTFOM_4$ is a special case with regard to repair rates. $FTFOM_4$ is evaluated by using a repair rate of μ = 0.99 h^{-1} (highly frequent repairs, corresponding to repairs every 1.01 h of operation, representing a limiting case) for the $MTTF_{HR}$ term and μ = 0.0 h^{-1} (no repairs) for the $MTTF_{NR}$ term.

3.1.3.4 Derating and Mass Multiplier Factors

Derating factors *OF* and *KVAOF* have been calculated for each topology using the provided formulas and the established component ratings. These derating factors are used to calculate $FTFOM_6$ and $FTFOM_7$. A summary of performance derating factors is provided in Table IV. The *KVAOF* metrics reflect the 50% voltage derating for topologies capable of full output torque after one fault for the direct redundant and two-module topology, and after two faults for the four-module topologies, as discussed previously. Calculation of $FTFOM_5$ requires the estimation of mass differences between the studied FT topology and the baseline configuration. The baseline mass was estimated by Jahns and Swanke (2024). The estimated power electronics masses are m_{pe} = 6 kg and machine mass m_{em} = 14 kg. Design-specific mass multiplying factors *MMF* and *DMF* are included in Table IV.

3.1.3.5 Case Study Results

Case study FT-FOM metric values have been calculated using the failure rates, stress factors, derating factors, and mass multiplier values described in the preceding subsection. For this discussion, four of the seven metrics that best highlight the reliability FOM trends (FT-FOMs 1, 3, 4, and 5) are plotted in Figure 7. The full set of calculated FT-FOMs are also summarized in Table V for completeness. The bar charts of Figure 7, showing FT-FOM values, exhibit some notable differences between the topologies that are helpful for highlighting their individual strengths and limitations. Some of the differences between the topologies that become apparent from these FT-FOM bar charts will be discussed here.

1. The five-phase topology exhibits the worst FOM metrics, particularly for $FTFOM_1$, because its fault coverage is insufficient to realize significant MTTF benefit for the motor drive system.
2. The direct redundant topology achieves a significant MTTF improvement, as observed in $FTFOM_1$, due to its improved fault mode coverage compared with the five-phase topology; this can be further improved with higher repair rates since it is the least saturated of the five technologies by the SPF rate, as indicated in $FTFOM_3$. However, it is disadvantaged by a mass penalty, as compared to the three modular machine topologies, that is reflected in its lower value of $FTFOM_5$.
3. Comparing the two- and four-module MMD topologies without the enhanced SPF rate, the four-module MMD topology achieves significantly higher values of both $FTFOM_1$ and $FTFOM_5$, highlighting its advantages in terms of higher drive system MTTF and reduced mass penalty. This suggests the desirability of increasing the number of modules in the MMD topology to more than two.
4. The value of $FTFOM_3$ for the four-module topology without the enhanced SPF rate is 1.0, which indicates that the SPF rate is limiting its ability to achieve still higher values of drive system MTTF. This is confirmed by the dramatic increase in the $FTFOM_1$, $FTFOM_4$, and $FTFOM_5$ values that results from reducing the SPF rate for the four-module topology.

TABLE IV.—SUMMARY OF DERATING FACTORS AND MASS MULTIPLIER FACTORS

Topology	Derating factors		Mass multipliers		Notes
	OF	*KVAOF*	*MMF*	*DMF*	
Five-phase design	1.25	1	1.25	1.59	Added devices: 4 devices, 4 gate drives, 2 current sensors
Direct redundant	2	2	4	2	Added devices: 6 devices, 6 gate drives, 3 current sensors, 1 controller, 1 capacitor Subjective multiplier of 2 applied to MMF to reflect gearbox mass, multiple housings, cooling loops, etc.
Two-module MMD	2	2	2	2	Added devices: 6 devices, 6 gate drives, 3 current sensors, 1 controller, 1 capacitor
Four-module MMD	1.33	2	1.33	4	Added devices: 18 devices, 18 gate drives, 9 current sensors, 3 controllers, 3 capacitors

Taken together, the results of this FT-FOM case study reinforce previous observations (Swanke, Zeng, and Jahns 2021) about the most promising approach to overcoming the challenging motor drive reliability gap for urban air mobility applications that was identified by Darmstadt et al. (2021). More specifically, these FT-FOM values support the conclusion that the path to achieving the highest possible drive system reliability consists of maximizing the repair rate (i.e., fast response to faults resulting in repair) and concurrently suppressing all SPFs using the most effective available techniques, such as health monitoring and redundancy. The results also suggest that increasing the module count in modular drives to a value higher than 2 is desirable for reducing the overrating factors and associated mass penalty. Using the MTTF as the measure of reliability, the FT X4-MMD+ configuration was determined to have ~750 times greater reliability as compared to the non-FT baseline standard configuration with favorable overrating factors and a modest mass penalty.

3.2 Time-Inhomogeneous Markov Chain Modeling of Fault-Tolerant Systems

In Section 3.1, a time-homogeneous motor reliability model was developed and applied. Certain motivations led to the development of a second motor reliability model, as described in this section. The type of model developed in Section 3.1 requires a significant approximating assumption, namely, all components' failure rates are approximated as constant with time. An equivalent statement is that all components' failure rate distributions are exponential distributions. Nelson (1990) discusses the widespread use of the exponential distribution for reliability modeling. He acknowledges that its use can yield useful (approximate) results, and the mathematical simplicity of application is appealing to many. But he cautions about misuse of the exponential distribution. He judges that only 10% to 15% of products are adequately described with an exponential distribution, and he recommends the Weibull distribution as a better alternative. With some study of the literature, it became clear that a reliability model for a FT motor could be developed while adopting Nelson's suggestion, that is, while using the Weibull distribution as the description of component failure time distribution. Such a model is described in this section and applied to a case study.

Weibull distributions are commonly and effectively used to describe the failure-time distributions of many types of mechanical and electric components, such as electrical insulation, bearings, gears, fans, integrated circuit packs, shock absorbers, and more (Meeker and Escobar 1998). For the Weibull distribution, the propensity for failure of any one component

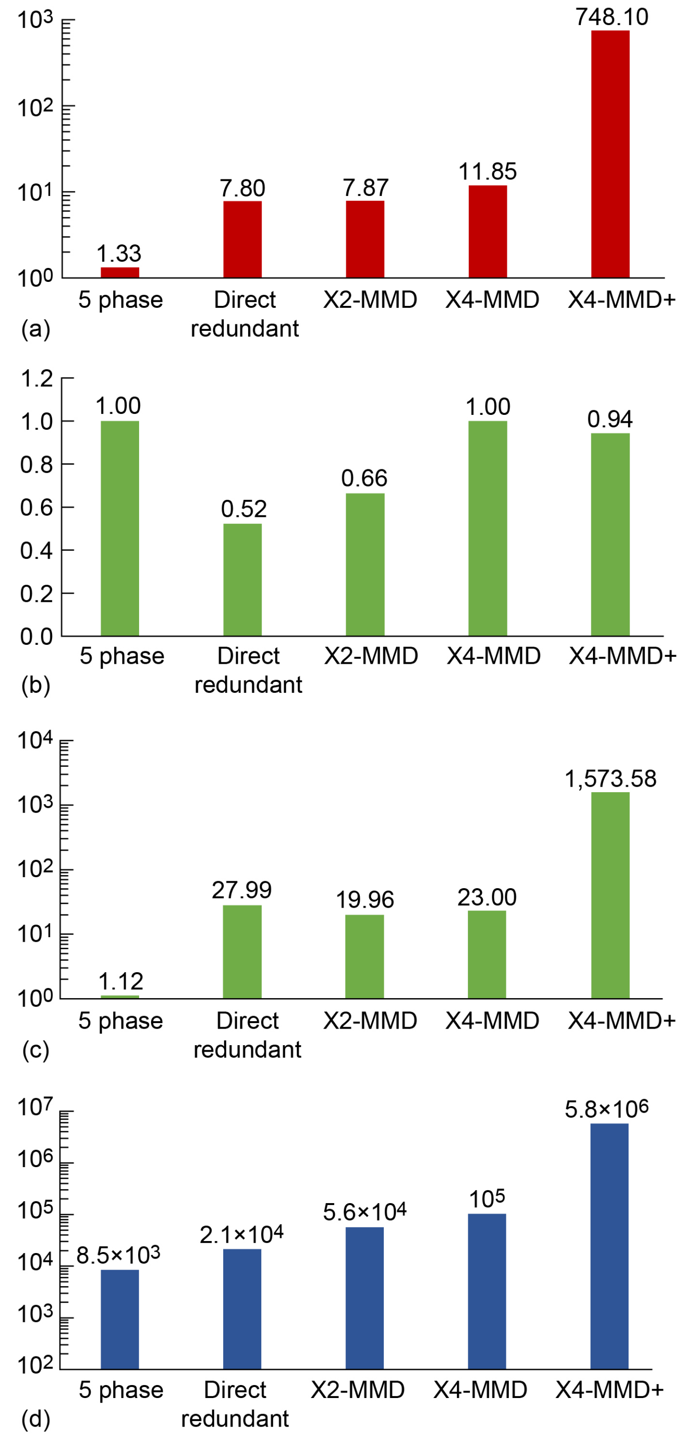

Figure 7.—Some FOMs from case study results for five-phase (5-phase), direct redundancy through a gearbox (Direct red.), two-module MMD (X2-MMD), four-module MMD (X4-MMD), and four-module MMD with reduced SPFs (X4-MMD+) (adapted from Jahns and Swanke 2024). (a) $FTFOM_1$. (b) $FTFOM_2$. (c) $FTFOM_4$. (d) $FTFOM_5$.

TABLE V.—SUMMARY OF CASE STUDY RESULTS

FTFOM		Five phase	Direct redundant	×2 MMD	×4 MMD	×4 MMD+
1	$MTTF/MTTF_{std}$	1.33	7.80	7.87	11.85	748.10
2	$\Delta MTTF/MTMF$	0.13	6.45	5.67	7.29	541.50
3	$MTTF/MTTSPF$	1.00	0.52	0.66	1.00	0.94
4	$MTTF_{HR}/MTTF_{NR}$	1.12	27.99	19.96	23.00	1,573.58
5	$\Delta MTTF/\Delta kg$	8.5×10^3	2.1×10^4	5.6×10^4	1.0×10^5	5.8×10^6
6	$\Delta MTTF/F$	4.3×10^4	5.6×10^5	5.6×10^5	1.3×10^6	9.2×10^7
7	$\Delta MTTF/KVAOF$	5.4×10^4	5.6×10^5	5.6×10^5	8.9×10^5	6.1×10^7

at any instant in time has a closed-form solution. However, to determine the reliability of a system of such components, a numerical solution is needed because there is no known general closed-form solution. In 2013, Jackson published a novel approach combining Markov and Weibull models, and the motor model developed herein follows Jackson's approach and guidance. In the text to follow, the development of the second reliability calculation procedure for a FT motor is described in detail, step by step.

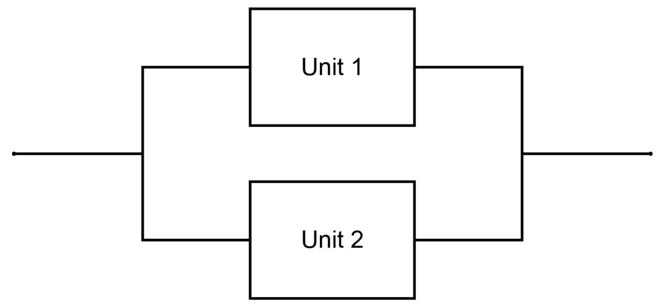

Figure 8.—Block diagram of two-element redundant system.

3.2.1 Combination of Markov and Weibull Modeling

The first step taken to combine Markov and Weibull modeling for a FT motor was to study the simplest possible redundant system: a two-element, fully redundant system, depicted in block diagram form in Figure 8. To study the system reliability, the system is modeled as a four-state Markov chain per Figure 9. The four state descriptions are as follows:

- State 1: Both units are operating.
- State 2: Only unit 1 has failed.
- State 3: Only unit 2 has failed.
- State 4: Both units have failed.

State 4 is considered system failure, whereas any of states 1, 2, or 3 is considered as system success.

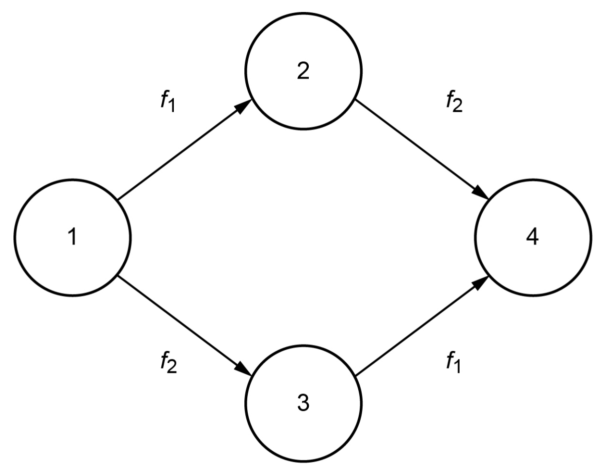

Figure 9.—Markov diagram of two-element redundant system.

In the Markov diagram of Figure 9, the transition paths are noted and labeled. The label "f_1" is intended to denote that unit 1 fails during the Markov chain "step" or "epoch," and so the associated transition occurs. If one wished to develop the set of differential equations for the system (Eq. (19)), then f_1 is the hazard rate for unit 1 (Eq. (5)). In this work, the finite-difference form of equations is determined from the Markov diagram (Eq. (22)), and thus f_1 is the probability of transition (Eq. (6)). The state memberships and the probabilities of transition are all functions of time. The Markov transition matrix **P** (see Eq. (22)) can be determined step-by-step with the aid of the Markov diagram as follows: (1) build the matrix column-by-column; (2) for each column, note the arrows exiting the associated state number, and place the probability of transition into the matrix per the row number corresponding to the destination state; and (3) assign the diagonal term such that the sum of all elements of the column equals 1. The diagonal term represents the probability of remaining in the same state (such a term is not directly depicted in the Markov diagram but must be accounted for). The sum of the terms of each column must equal 1, because the total probability of remaining in the state or transitioning to another state must sum to 1.

The probabilities of transition represented by f_1 and f_2 in Figure 9 are functions of time. To solve the matrix equations numerically for one Markov epoch that begins at t_1 and ends at t_2, the transition probability is approximated per Equation (6) as the product of the time increment $\Delta t = (t_2 - t_1)$ and the value for the associated hazard function evaluated at the epoch midpoint $((t_1 + t_2)/2)$. This formulation is the equivalent of solving the differential equations via Euler's midpoint formula.

Following the approach of Jackson (2013), an example study was conducted for the case in which the failure time distribution of each unit followed a Weibull distribution having a shape parameter equal to 1.0 and a scale factor equal to 5.0 yr. The time-marching time step Δt was selected as 1/500 yr. The shape parameter was selected as 1.0, because in such a case an exact analytical solution is available, making it possible to verify the numeric code and to assess numerical error. The initial condition imposed was that one population of units were all in state 1 at global time $t = 0$. At each time step beginning at time t, the values of the transition matrix are calculated, then matrix multiplication yields the state membership vector at time $t + \Delta$, and this becomes the initial state membership vector for the next time step. At any time, the sum of membership in states 1, 2, and 3 represents the reliability of the system, that is, the fraction of the total population that is in successful operating status.

A numeric code was developed, and solutions obtained, for 500 time steps, representing 1 yr of operation. Solutions obtained matched those reported by Jackson (2013). The result from the numeric code was a reliability of 0.967118324, and the result by analytical formula was 0.96714146, thus the numeric error equals 2×10^{-5}. Extending the simulation for 10-yr operation using the same time step size yielded the results of Figure 10 (for system reliability) and Figure 11 (for percent error relative to the exact solution). The percent error is small, for all practical engineering purposes.

3.2.2 Selection of Time-Step Size

To guide the selection of an appropriate time step for a FT motor model, solutions were obtained for the Markov model of Figure 9 for three time-step sizes; results are provided in Table VI. It is evident that selection of Δt as 1/2500 of the scale parameter (results of row 2) provides sufficient accuracy for engineering purposes. A population of eVTOL motors used for 500 flights/yr and operating for 10 yr serves as a supporting example. If one selects a time step per row 2, each time step represents a single flight. It is likely that motors will have higher usage rates and higher reliability requirements than this example, and so it is judged that one flight is a sufficiently small time step for Markov-Weibull chain numerical solutions for eVTOL reliability studies.

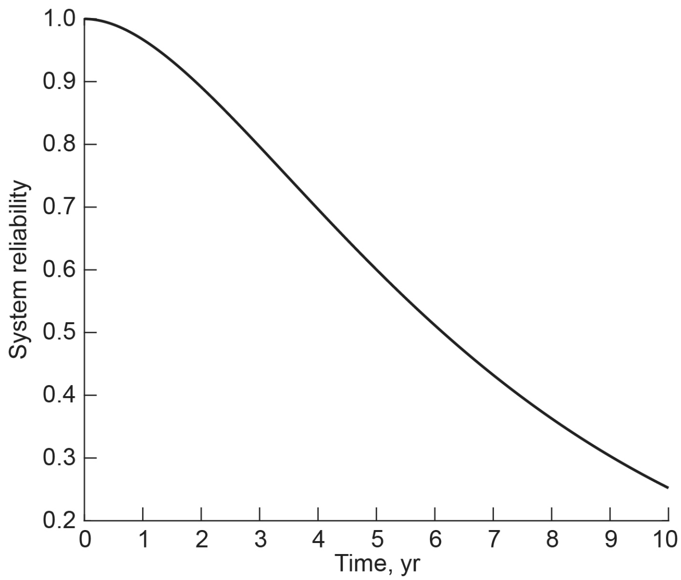

Figure 10.—System reliability for two-component redundant system by numeric solution.

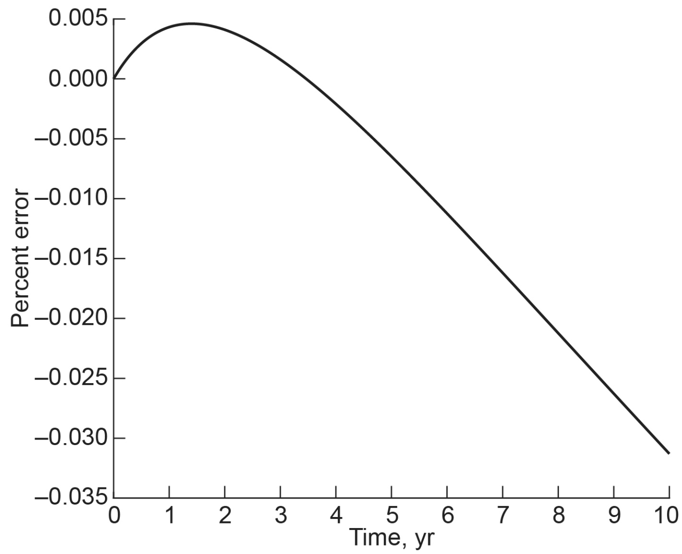

Figure 11.—Percent error of numeric solution of Figure 10 relative to exact analytical solution.

TABLE VI.—RESULTS OF TIME-STEP SIZE STUDY

Δt, yr	Simulation cycles required, no.	Percent error at $t = 10$ yr	Ratio of Weibull scale parameter to Δt
1/100 = 0.01	1,000	–0.1566	5/0.01 = 500
1/500 = 0.002	5,000	–0.0312	5/0.002 = 2,500
1/2500 = 0.0004	25,000	–0.0062	5/0.0004 = 12,500

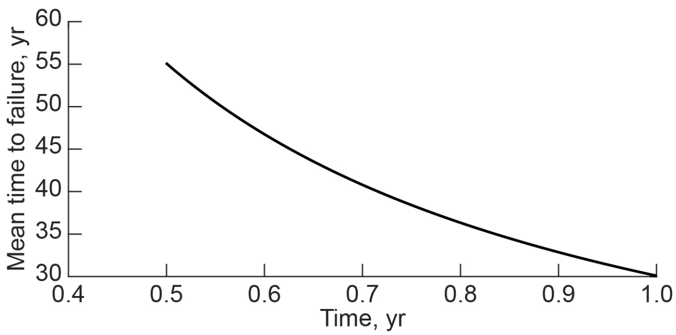

Figure 12.—Trend of mean time to failure with time, up to 1 yr total.

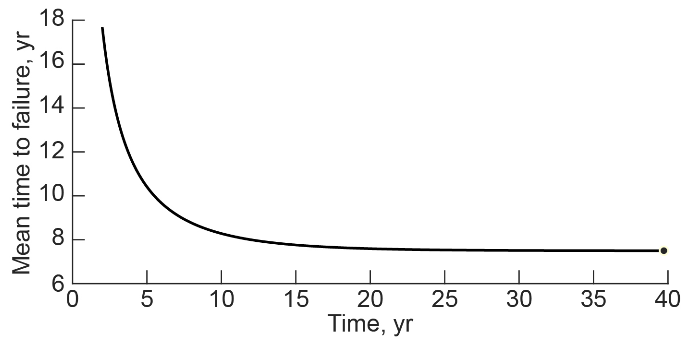

Figure 13.—Trend of mean time to failure with time, up to 40 yr total.

3.2.3 Influence of Scheduled Retirement Time

The influence of a scheduled retirement time on system reliability can be studied using the combined Markov-Weibull model. The redundant system of Figure 8 was modeled and solved for an operating time of 1 yr. Each individual unit had a *MTTF* of 5 yr. Per Figure 12, the system *MTTF* decreases as operating time is accumulated. After 1 yr, the system *MTTF* is approximately 30 yr, even though the *MTTF* of each component is only 5 yr. Further extending the analysis to operation for 40 yr yields the *MTTF* results of Figure 13. The long-term *MTTF* of the system is only 7.5 yr. The plots of Figures 12 and 13 highlight that for redundant systems, using a small scheduled retirement time can result in a high system-level *MTTF.* In this example case, the system-level *MTTF* can be 6 times the component-level *MTTF* by using a 1-yr retirement. Of course, such an approach would have a large economic expense. Still, in concept, the selection of a scheduled retirement time for a FT motor can contribute toward meeting safety requirements, and the combined Markov-Weibull tool can be used to study such influence.

3.2.4 Influence of Weibull Shape Parameter

The results of Figure 10 to 13 were obtained while imposing a Weibull shape parameter equal to 1.0 because an exact solution could also be obtained. This allowed for code verification and assessment of an appropriate time-step size. However, a Weibull shape parameter equal to 1.0 has a constant hazard function, so it is not representative of the failure distribution of most components that have an increasing hazard function. The behavior of a FT redundant system as represented by Figure 8 was studied using the Markov-Weibull model while varying the Weibull shape parameter. In all cases, the median lifetime of a unit was 3,500 h. The characteristics of the Weibull distributions are provided in Figure 14. Solutions were also obtained for a nonredundant one-module system while applying Weibull theory scaling laws to account for resizing of the single-unit-equivalent system. Results of this study, provided in Figure 15, illustrate the effectiveness of redundancy to improve system reliability. Note that the relative reliability improvement depends on both operating time and value of the Weibull shape parameter.

3.3 Markov-Weibull Model of eVTOL Concept Motor

In Section 3.1, various FT motor concepts were studied using a time-homogenous Markov model, and an integrated modular motor drive (IMMD) concept with reduced SPF modes (referred to as "MMD+") was shown as a promising concept for high reliability. In Section 3.2, methods were developed and example studies conducted for a generic FT system using a combined Markov-Weibull time-inhomogeneous model. In this section, the time-inhomogeneous Markov-Weibull model method is developed and solved for a MMD+ type concept motor. The example motor to be analyzed is described in detail by Tallerico, Smith, and Chapman (2023). The motor concept is based on the works of Swanke (2023) and Jahns and Swanke (2024). The motor topology, depicted in Figure 16, has four modules, and the design includes features to maximize galvanic, magnetic, and thermal isolation between phases and modules in the machine.

(a)

Shape	Scale	Median	Mean
1.0	5,050	3,500	5,050
1.5	4,469	3,500	4,034
2.0	4,204	3,500	3,726
3.5	3,886	3,500	3,497

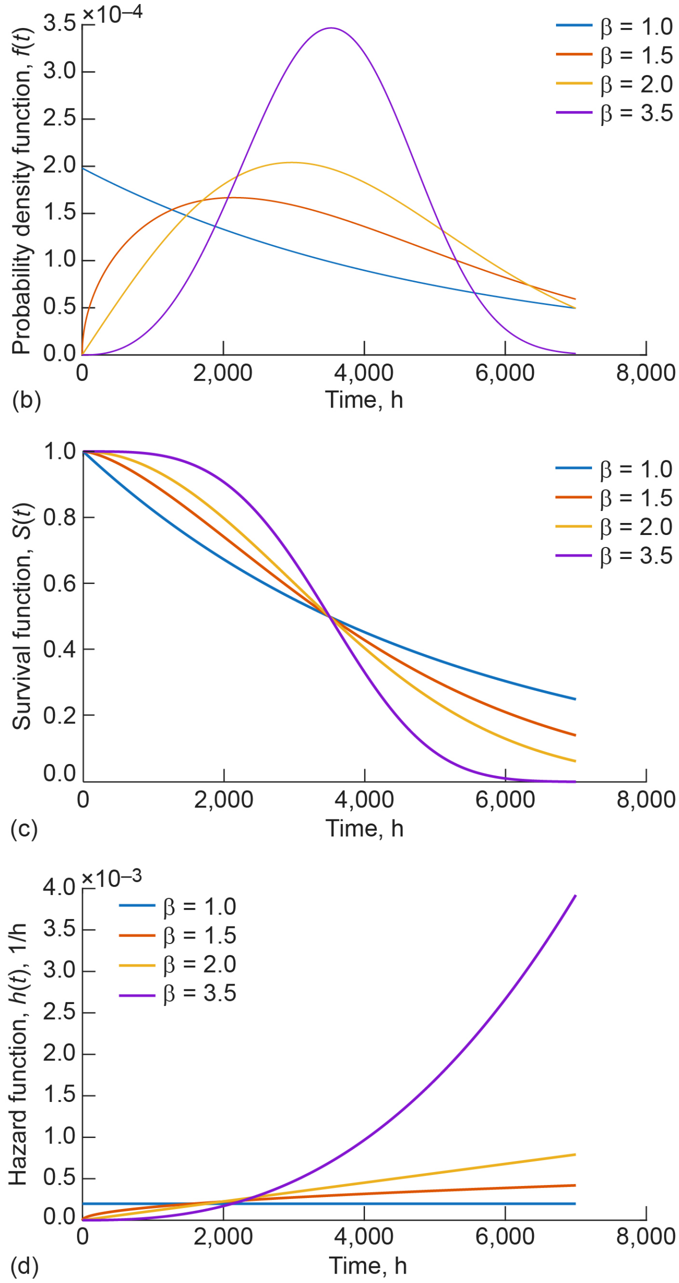

Figure 14.—Properties of Weibull distributions used for case study results of Figure 15. (a) Parameter values and properties. (b) Probability density function. (c) Survival function. (d) Hazard function.

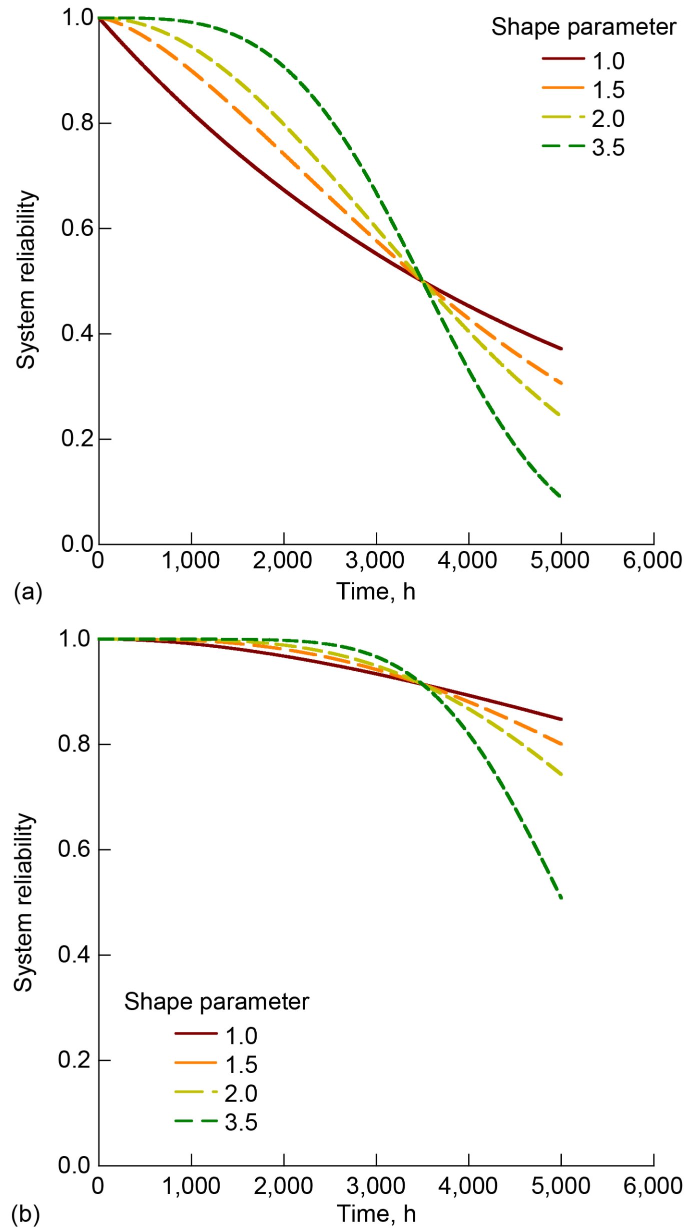

Figure 15.—System reliabilities as functions of time and Weibull shape parameter. (a) Results for one-module (no fault tolerance) system. (b) Results for two-module (FT) system.

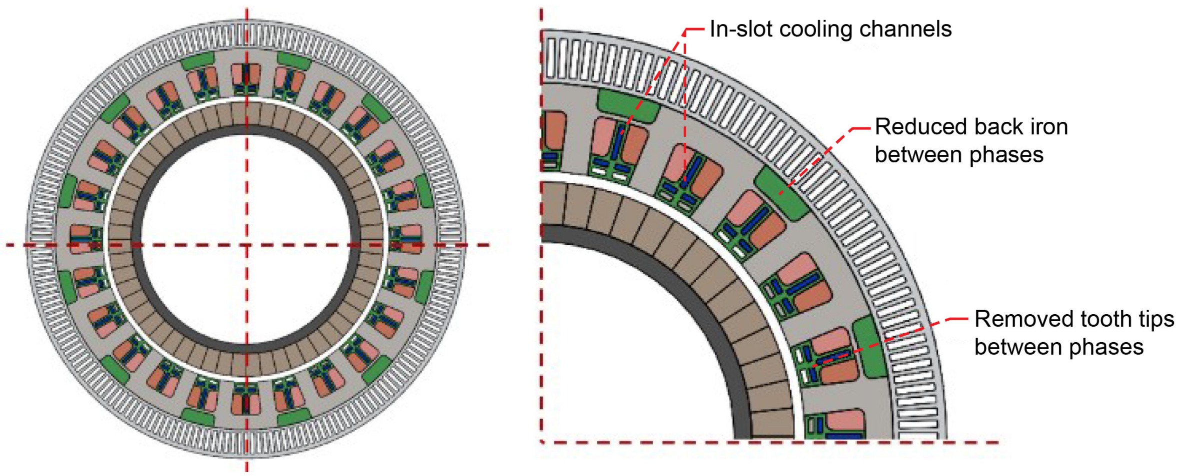

Figure 16.—FT motor concept for Markov-Weibull reliability study (Tallerico, Smith, and Chapman 2023).

3.3.1 Modeling of Electric Motor Failure Modes

Permanent-magnet synchronous motor faults can be categorized into three main categories, namely, electrical, mechanical, and magnetic faults (Chen et al. 2019). Proper design, qualification, and quality production of aviation-class motors should eliminate some failure modes that are commonly observed in industrial motor applications. However, given that the aircraft application requires small mass, not all long-term failure modes can be assumed to be eliminated. It is generally accepted that the reliability of high-performance motors will be limited by the eventual occurrence of stator winding faults and bearing fatigue faults. That is, given the power density requirements of aircraft motors, these faults can be expected to have a low but nonzero probability of occurrence over the service lifetime of the motor. The FT motor concept is designed for continued operation after a fault occurs, with a high probability of operating and delivering propulsive power for the duration of the flight, after which a replacement and repair action can be completed. The Markov-Weibull model described in the following text considers stator winding faults and bearing fatigue faults, but motor demagnetization faults are not modeled. This approach is considered justified per the findings of Sjökvist (2014) concerning permanent-magnet machines; Sjökvist concluded that rotors can be designed to eliminate demagnetization faults.

3.3.2 Flight Mission and Winding Thermal Profiles

The example motor design to be analyzed is a from a study detailed in Tallerico, Smith, and Chapman (2023). The assumed flight mission profile is a single flight of the two-flight mission from Silva et al. (2018). It is assumed that in the event of a motor winding fault, the vehicle will fly at cruise power to a landing location and hover to land. As a worst case, winding faults are assumed to occur at the top of climb, when the motor is already at its hottest condition. The motor's thermal profile (the temperature of the winding hotspot during the flight) was determined by the method described in Tallerico et al. The motor design optimization process limited the maximum shear stress in the windings to be less than 13 MPa. Two thermal profiles were determined. One profile was determined for a nominal mission with all modules operating; the second profile was determined for a flight in which one module experiences a fault at top of climb and the remaining three modules must increase power output to compensate and deliver full requested power. The winding temperature profiles are depicted in Figure 17.

3.3.3 Technique for Simplification of Markov Diagrams

A Markov chain diagram for a four-module FT motor was developed by Swanke and Jahns (2022) and is shown in Figure 18(a). In this diagram, a fault of a stator quadrant is indicated by an overbar (e.g., a faulted quadrant A is indicated by $\overline{\mathrm{A}}$). Solid lines indicate stator module fault transition paths and associated rates. Dotted lines indicate paths and rates for single point of failure (failure modes other than the stator). The healthy state is H, and the failed state is FS. The Markov diagram can be simplified if one makes the modeling assumption that all four modules belong to the same population. That is, the propensity to failure is no different for module A versus module B, or the others. Reliability block diagrams are simplified by recognizing parallel and series reliability structures. From an operational reliability block diagram perspective, the modules act as a "2 of 4" parallel structure, that is, the system operates even if two of four modules are faulted. However, from a Markov chain transition path perspective, the four modules operate as a series structure, because the event of one fault results in transition to another state. Using this series-structure idea, the Markov diagram may be simplified as shown in Figure 18(b). FT1 is a state of one module failed, and FT2 is a state of two modules failed. The failure transition rates for a single module must be adjusted according to the number of modules still at risk when creating the transition matrix diagram Figure 18(b).

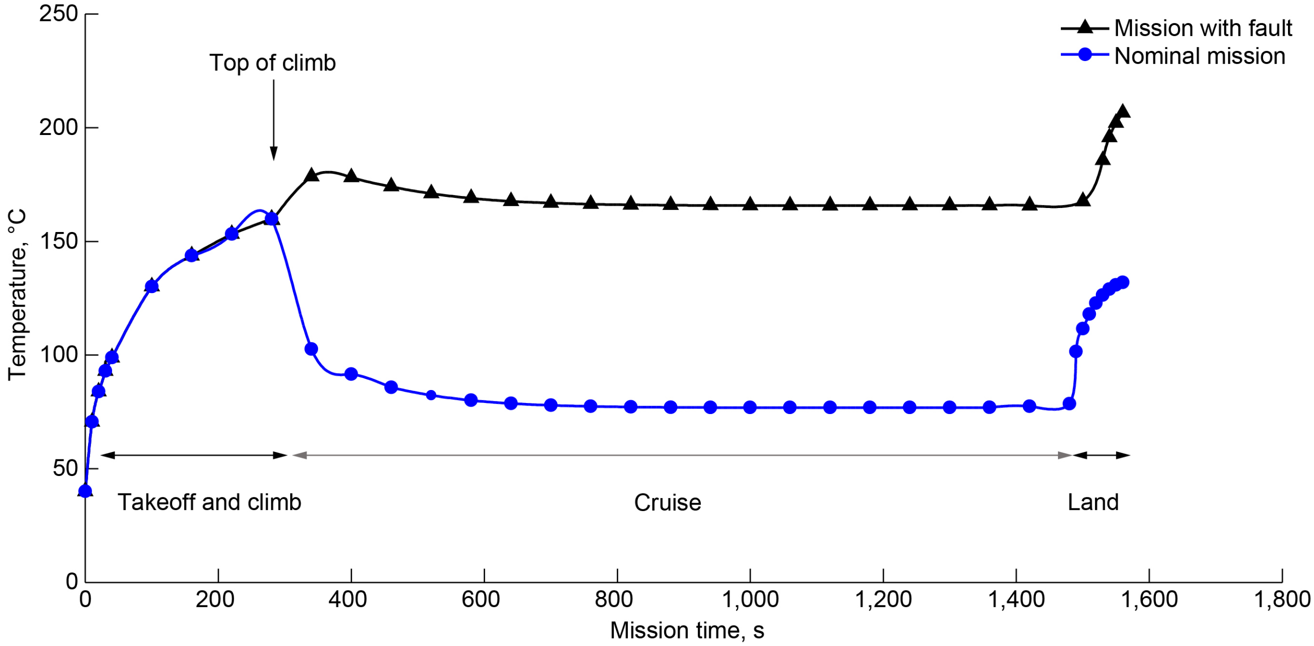

Figure 17.—Thermal profiles of winding hotspot for nominal mission (circle symbols) and mission with one module becoming faulted at top of climb (triangle symbols).

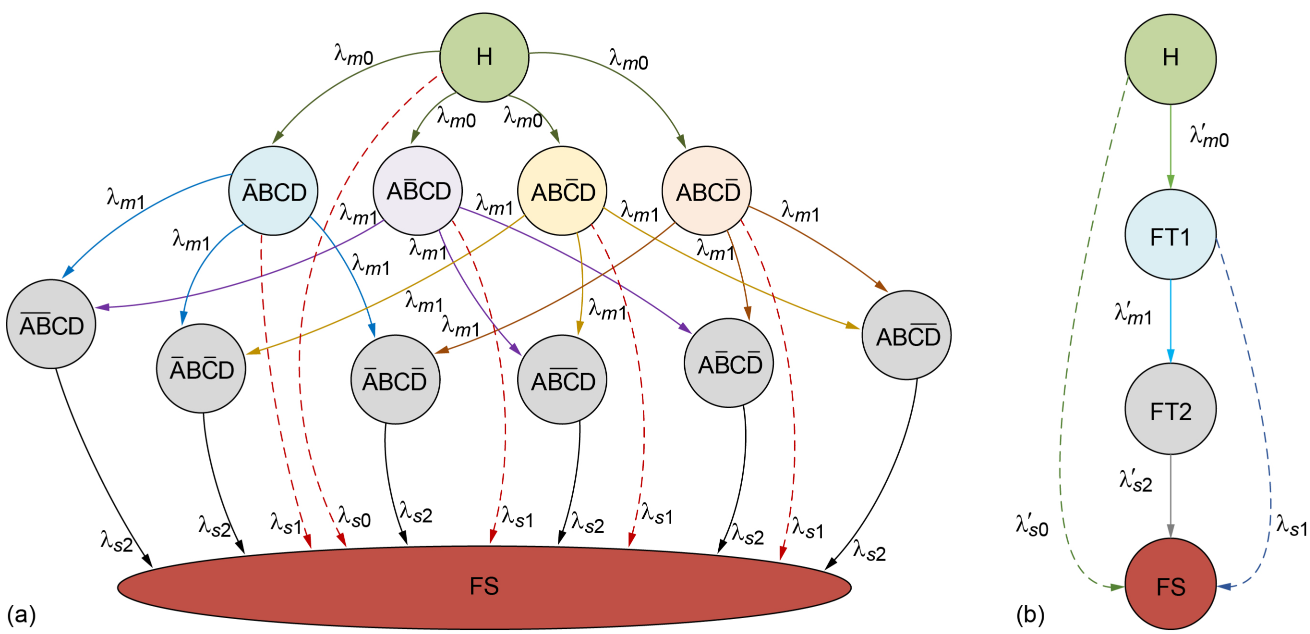

Figure 18.—Four-module Markov chain diagram that allows two failed modules before IMMD failure. Repair transitions are not shown to minimize diagram complexity. (a) Full diagram of Swanke and Jahns (2023, adapted). (b) Diagram after simplification via series-structure concept.

3.3.4 Linked-Chain Markov-Weibull Model

A Markov-Weibull model was created for the concept eVTOL FT motor. A new method termed “linked chain” was developed and implemented to customize the Markov-Weibull model for this study. For eVTOL missions, it was shown previously that modeling each eVTOL flight as a single Markov epoch was a sufficiently small-sized time step for accuracy of the time-stepping numerical solution. The implemented model was devised to be modular and easily expanded. The implementation introduces a new concept termed “linked Markov chains.”

The idea for the linked-chain approach being introduced herein was inspired by the medical modeling community, where tunneling states and nested models are introduced into constant-transition rate Markov chains to model time-dependency of medical treatments (Shah et al. 2012; Alarid-Escudero et al. 2023). A Markov tunnel is typically a short-length chain of temporary states. Membership in a temporary state is limited to one Markov epoch. A series of such temporary states is termed a tunnel. The newly devised linked-chain approach includes creation of separate Markov chains for each faulted state, and each faulted state is resolved to a final absorbing state at the end of an individual mission. This approach simplifies model and numerical code development, and there may be value in studying the properties of a particular linked chain separately. For example, the first of the chains (Figure 19(a)) could be simulated once and results stored. Operational options could then be explored using these results as inputs to other linked chains with different structures. This approach creates building blocks whereby different subject matter experts can improve the realism and fidelity of individual linked chains. Of course, the behavior of the system requires bringing all linked chains together and completing appropriate simulations.

Steps 1 and 2 of the linked-chain model are discussed in the following subsections.

3.3.4.1 Linked-Chain Model Step 1: Define Faulted States

Faulted states are defined in the first Markov chain, to be later linked to additional chains. The first Markov chain does not attempt to resolve whether a motor fails from a faulted state before the end of mission; rather, it only identifies all possible fault states. As was described earlier, the implementation herein considers that two types of faults cannot be eliminated by design and qualification, namely, that stator degradation occurs with usage and time and can eventually lead to a winding fault, and similarly, that bearing material fatigue can accumulate and eventually precipitate a bearing spalling fault. The first of the implemented linked chains is depicted in Figure 19(a). The state definitions of Figure 19(a) are defined as follows:

1. H is a healthy state with no known faults.
2. FT-S is a fault mode of the stator, that is, because of an open or short circuit in a winding, one of the four quadrants of the four-module stator is powered off, and the power to the remaining three modules is boosted to continue delivering full demanded power.
3. FT-B is a fault mode of a bearing. A bearing has become spalled and so is considered not fit for service for the next flight.

In Figure 19(a), an arrow is depicted as originating from and returning to a healthy state. However, there exist no pathways from other states returning to the healthy state H. The implemented model is one for a cohort of a large population. In this model, units may be retired from service after a flight, as will be determined using other linked Markov chains. New or refurbished units are not added back into the cohort population to replace failed units. Therefore, the model presented herein does not support operational issues such as anticipating and scheduling spare part needs or calculations of fleet availability; development of a model to answer such questions for systems with time-inhomogeneous components is beyond scope of this effort.

In diagram of Figure 19(a), there are no SPF modes. However, if one were to model a topology with a SPF mode, the transition path for the SPF mode to the failure state would be added to the diagram of Figure 19(a).

3.3.4.2 Linked-Chain Model Step 2: Define Faulted State Resolutions

The second step of the linked chain modeling process is to create additional Markov diagrams, one for each faulted state, that result in resolution of each such state. The two additional Markov diagrams for the example implemented model are provided in Figure 19(b) for resolution of the faulted modular winding state FT-S and in Figure 19(c) for resolution of the spalled bearing fault state FT-B. These Markov chains have destination states R-S and FS. R-S means “remove from service”; that is, the mission was completed with the motor providing demanded power, and then the motor was removed from service. FS is the failed state of the motor unable to deliver demanded power during the flight. In the terminology of Markov modeling, the states R-S and FS are “absorbing states.” For an absorbing state, there is no possibility to transition to another state.

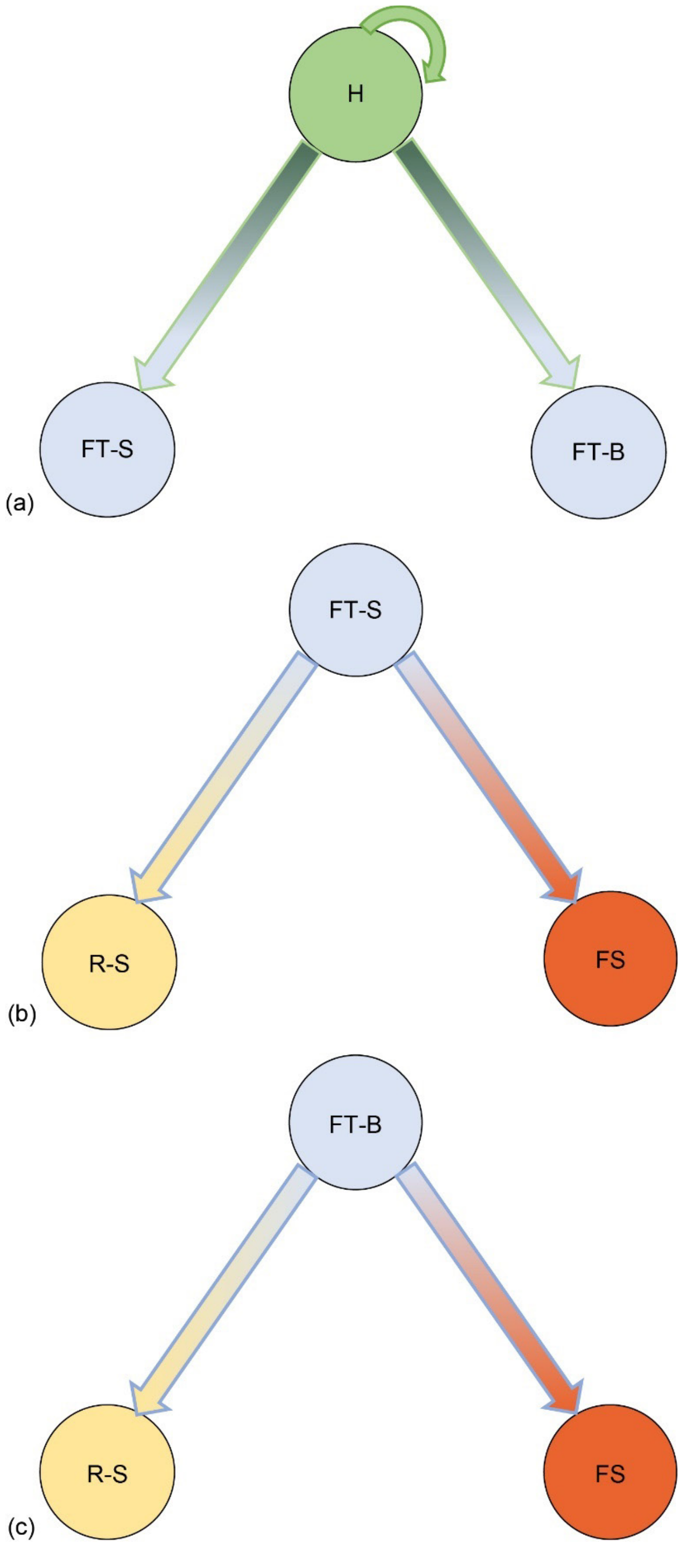

Figure 19.—Linked chain diagrams of a Markov model of eVTOL motor reliability. (a) Transitions to faulted states. (b) Transitions from faulted stator state to removal from service or failure state. (c) Transitions from faulted bearing state to removal from service or failure state.

3.3.5 Arrhenius-Weibull Model of eVTOL Concept Motor Windings

The newly proposed Markov linked-chain motor model is a cohort model using a finite-difference equation formulation (Eq. (22)). The terms of the transition matrix are conditional probabilities that can be formulated as approximately equal to the hazard function multiplied by a time increment (see Eq. (6)). Per discussion of Table VI, sufficient numerical accuracy can be achieved when selecting the time increment for the cohort model to be one flight. To calculate the hazard function, a probabilistic life model is required. For the motor windings, the life model implemented is an Arrhenius-Weibull thermal aging relation combined with the linear damage rule, modified by an adjustment factor for thermal cycling. The Arrhenius-Weibull and linear damage equations were introduced in Section 2.0. To apply the model, four constants must be selected by the analyst. This section describes the selections of the constants and associated calculations needed to complete an example calculation of the reliability of the eVTOL concept motor.

The Arrhenius-Weibull equation relates the thermal aging median lifetime (i.e., the 50th percentile) of the windings as a function of exposure to constant temperature. The relationship plots as a straight line using appropriate plotting scales, and two parameter values define the relationship. The literature was reviewed to guide selection of realistic parameters for the eVTOL concept motor. Figure 20 displays two Arrhenius relationships for motor windings from the literature. Madonna et al. (2019) tested twisted-pair wires, coils, and motorettes to assess the thermal lifetime. Of the three tested specimens, the motorettes are most like a stator coil. The tested motorettes were fabricated using a high-temperature class wire. The experimentally determined Arrhenius model for the motorette specimens is plotted using circle symbols in Figure 20. Griffo, Tsyokhla, and Wang (2019) tested stators from production motors by removing the rotors and subjecting the stators to constant-temperature exposure experiments to establish a baseline for thermal cycling experiments. The experimentally determined Arrhenius model for the stators is plotted using triangle symbols in Figure 20. In Figure 20, the slopes for the stators and the motorettes are similar. For the eVTOL concept motor, the Arrhenius model was selected to match the slope of the Figure 20 motorette data (Madonna et al. 2019). The second equation parameter for the Arrhenius equation was selected to match that of a typical thermal class A magnet wire. Thermal class A wire is a reasonable selection given the thermal profile experienced by the concept motor, per Figure 17. The selected parameters (for Eq. (16)) were $A = 2.6\times10^{-15}$ (h) and $B = 17{,}595$ (1/K). To implement the Arrhenius-Weibull model, a Weibull shape parameter must also be selected. For the implementation herein, a Weibull shape of 3.0 was selected as representative of

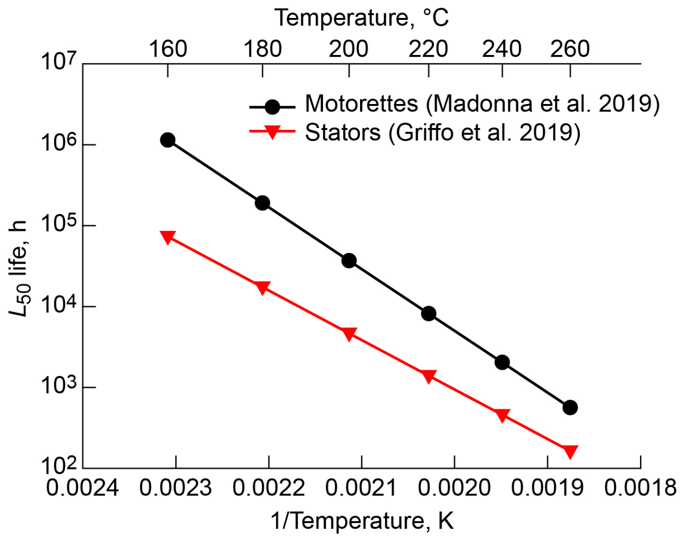

Figure 20.—Experimentally determined Arrhenius curves defining thermal lifetimes; typical results from literature.

data in the literature. A Weibull distribution with a shape parameter of 3.0 has a probability distribution function plot that resembles a bell-shaped Gaussian distribution, but the distribution is slightly skewed right.

To calculate the hazard function for the current Markov chain epoch (the current flight), the total cumulative thermal damage for all previous flights is required. The cumulative thermal damage is determined using the linear damage law as follows. First, the thermal profile is approximated by a stepwise profile, a series of constant temperature segments. The nominal mission thermal profile of Figure 17 was extended to include a motor cooldown after flight completion, and the profile was approximated as a set of constant-temperature segments (Figure 21). The thermal damage for each short constant-temperature segment is calculated using the Arrhenius-Weibull equation and linear damage rule, and then all damage is summed for the flight. The result of such calculation is depicted in Figure 22. Note that almost all the thermal damage occurs only for temperatures above 120 °C, and most of the damage occurs during takeoff. After transitioning to the cruise condition, the motor winding temperatures rapidly decrease, and thermal damage during the remaining cruise segment is negligible. A second thermal peak occurs during the landing phase near the end of mission, demanding more power than is needed during the cruise segment. The thermal damage during landing is small but not negligible. Thermal damage of the nominal flight is about a 1.8×10^{-7} fraction of the median lifetime. The damage calculation procedure was repeated for the faulted mode thermal profile of Figure 17, and it was determined that such a profile resulted in approximately 44 times greater thermal damage fraction relative to that of the nominal profile. Such a result is needed for calculation of Markov transition probabilities when the motor is operating in the stator-faulted mode, FT-S, of Figure 19.

The preceding paragraph calculates the damage using the classical Arrhenius model for the winding insulation lifetime. It is widely recognized that thermal cycling can have a large effect on the lifetime of motors. A motor that operates continuously at a given temperature tends to be more reliable than the same motor that operates intermittently and therefore experiences temperature cycles. Such an effect is usually termed a “thermal-mechanical aging effect.” Mechanical aging is thought to be mainly due to mismatch of materials’ coefficients of thermal expansion and nonuniform transient temperature variation within the motor. Thermal cycling therefore produces mechanical stress cycles and the associated damage. Although there is significant guidance for the design and testing of thermal cyclic effects for large and high voltage (>10 kV) machines, there is relatively little guidance for low-voltage machines. Griffo, Tsyokhla, and Wang (2019) conducted experiments that quantified a significant thermal cycling effect for a low-voltage class motor. Some stators were subjected to only constant-temperature aging while others experienced thermal cycling. The lifetimes of thermally cycled stators were significantly shorter than would be calculated via an Arrhenius pure thermal aging model calibrated using the constant-temperature experimental data. Griffo et al. proposed a modified linear damage thermal mechanical life model for which the total damage fraction DF is the summation of an Arrhenius thermal chemical damage term, DF_T, and a thermal cyclic damage term, DF_C, that is,

$$DF = DF_T + DF_C \tag{34}$$

$$DF_C = \sum\nolimits_{r,s} \frac{N_{\text{cycles}}\left(\Delta T_r, Tpeak_s\right)}{N_{r,s}} \tag{35}$$

and the term DF_T of Equation (34) is determined by the thermal profile duty cycle procedure described in the previous paragraph. The terms of Equation (35) are defined as follows: ΔT_r is the range of a thermal cycle, $Tpeak_s$ is the peak temperature, N_{cycles} is the number of cycles having the same range and peak, and $N_{r,s}$ is the number of cycles to failure for that given thermal range and peak, with $N_{r,s}$ determined empirically. From a set of dedicated experiments, Griffo et al. found that, at failure, the total damage fraction owing to thermal cycling, DF_C, ranged from 0.2 to 0.8. In the present work, the damage fraction is calculated using the Arrhenius thermal chemical damage fraction multiplied by a thermal cycling factor. A constant value of 2.0 was used for the thermal cycling factor for calculation performed herein. The code was written such that the cycling factor is an input parameter, and the factor value may be adjusted based on empirical evidence.

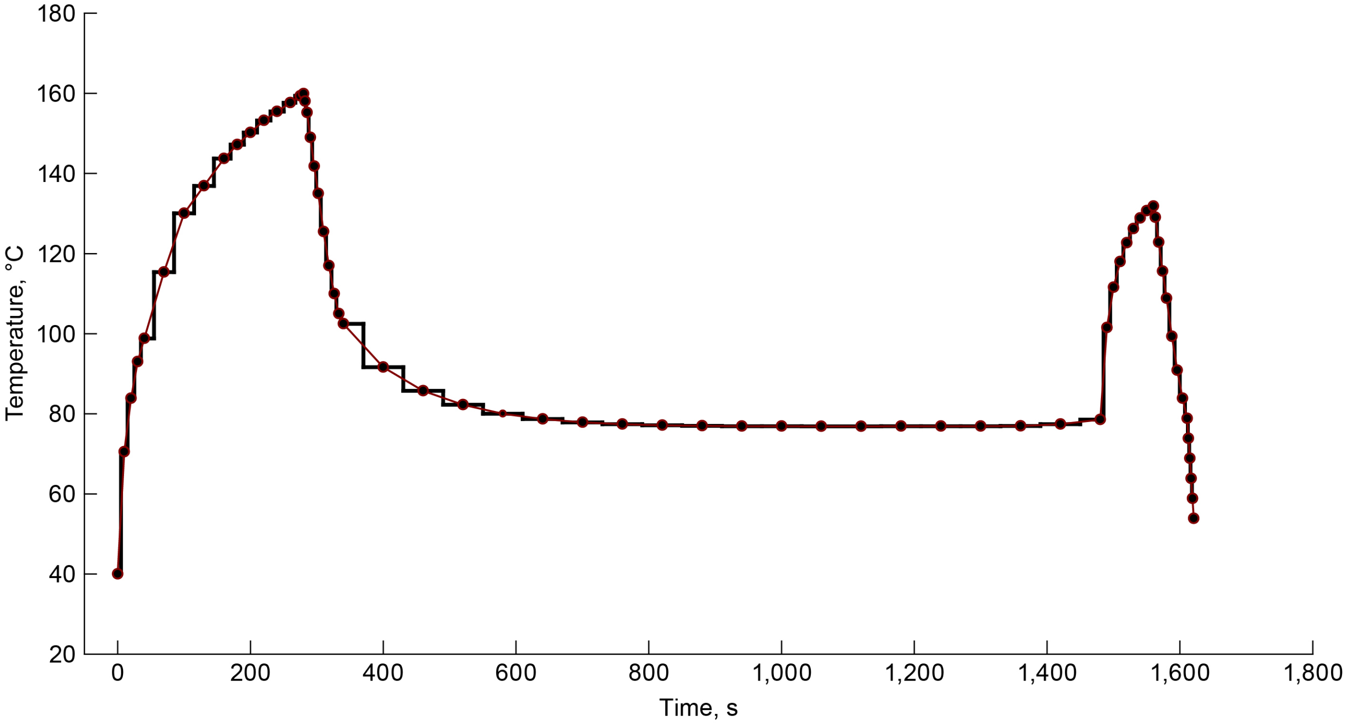

Figure 21.—Thermal profile of windings for nominal mission approximated using constant temperature segments.

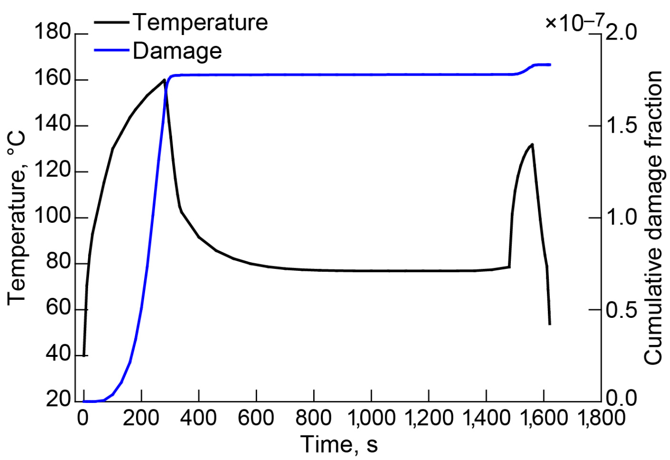

Figure 22.—Thermal profile of stator windings of eVTOL concept motor for nominal flight and cumulative thermal aging damage fraction as function of time.

3.3.6 Power-Weibull Model of eVTOL Concept Motor Bearings

In this work, it is assumed that all failure modes for bearings have been eliminated by proper design and qualification testing except for one failure mode, spalling of bearing by material fatigue. It is well accepted for aviation applications that the bearing lifetime will be limited by material fatigue resulting in a spall. Once a bearing spalls, the machine can typically operate for some time. The spalling creates loose debris that can be sensed by appropriate systems, such as oil debris monitors and chip detectors. The spalled condition also creates a change in the vibrations produced when operating the machine, and health and usage monitoring systems have been developed to detect the presence of a spall and call for a repair action.

In the present implementation for motor reliability, the bearing design and selection is assumed to have achieved a bearing spalling fatigue reliability requirement. The relationship of the probability of failure to the basic dynamic rating of the bearing is defined by a power law relation (Eq. (14)). A Weibull shape parameter for the failure distribution is also selected as an input parameter, establishing the Power-Weibull model. It is well established that Weibull shape parameters between 1.0 and 1.5 accurately describe most empirical data (Harris 1984). Example calculations to be presented used a Weibull shape factor of 1.5. The Markov chain model also assumes a health and usage monitoring process to detect the presence of a spall. Such a condition is considered as a faulted but not failed state. The details of the health and monitoring process are not modeled directly; instead, the capability of such a process is quantified as a success probability. Success of the health monitoring process is defined as the probability that removal and repair will be initiated prior to the spall progressing to such magnitude as to cause motor failure. The removal for cause may be triggered by maintenance checks, metal chip detection, lubricant analyses, vibration monitoring, temperature monitoring, or some combinations of such technologies and processes.

3.3.7 Reliability of eVTOL Concept Motor: Markov-Weibull Model Parameters and Results

In the preceding paragraphs, a time-inhomogeneous Markov-Weibull model was developed and described. There are nine numerical inputs for this model. In addition, the model requires as inputs two stator coil thermal profiles: (1) all four modules operational for the entire flight and (2) one stator module depowered after occurrence of a fault at the top of climb. For this study, the thermal profiles were per Figure 17. The model was exercised six times to explore the efficacy of the FT stator motor concept. In this study, the parameters related to the stator were kept fixed while the influence of bearing parameters was explored. This study assumed an average of five flights per day and a 10-yr service life, after which the motor is retired even if no fault has occurred. The average failure rates were calculated for both the FT eVTOL concept motor and for the same motor without the FT stator mode of operation (a stator fault is then considered a motor failure). The ratio of the average failure rates and ratio of *MTTF* for these two motors were also calculated. The average failure rates are directly comparable to the study of Darmstadt et al. (2019), and the *MTTF* ratio is directly comparable to the study of Jahns and Swanke (2024). Results of the calculations are provided in Table VII. Discussion of results follows.

Results for run 1. The first calculation was done to establish a baseline and to judge if the model produced reasonable results. The bearing reliability for the lifetime of the motor was 90%, and the bearing health and usage monitoring system (HUMS) success rate was set to 98%. The resulting failure rate for the motor with no fault tolerance was about 6×10^{-5} failure per flight hour. This result compares favorably as rough order to the 9×10^{-5} value used by Darmstadt et al. (2019) for failure modes and effects and fault tree analyses. For the motor designed with fault tolerance, the average failure rate improved (decreased) to about 5×10^{-7}. The improvement in reliability was on the order of 100 times by introduction of fault tolerance.

Results for runs 2, 3, and 4. These calculations were done to explore the influence of intrinsic bearing reliability on the overall reliability of the FT modular stator concept. For these calculations, the success rate of the bearing health and usage monitoring was set to zero success to highlight and quantify the influence of inherent bearing reliability. Bearing reliability can be increased by increasing bearing size and thereby decreasing bearing stress. No attempt was made to estimate the mass increase required to improve bearing reliability. The bearing reliabilities were 0.9, 0.999, and 0.9995, respectively, for runs 2, 3, and 4. The value 0.9995 was selected as a practical but perhaps upper-bound reliability. The value 0.9995 is required for NASA space mechanisms (NASA-STD-5017B). The study's results show that for the motor without fault tolerance, motor reliability did improve, albeit modestly, as the individual bearing reliability was increased. When the improved bearing reliability was increased by the same amounts for the FT motor concept, the improvement was more significant, with average failure rate decreasing from about 3×10^{-5} to 2×10^{-7}, an improvement of average failure rates by a ratio of over 200. This set of calculations highlights that all aspects of the motor must have high reliability or redundancy, otherwise the full value of FT features will not be fully realized.

TABLE VII.—RELIABILITY CALULATION RESULTS USING MARKOV-WEIBULL MODEL

	Run number	1	2	3	4	5	6
Inputs	Number of cycles (flights) for motor retirement	18,460	18,460	18,460	18,460	18,460	18,460
	Arrhenius constant *A*	2.61×10^{-15}	2.61×10^{-15}	2.61×10^{-15}	2.61×10^{-15}	2.61×10^{-15}	2.61×10^{-15}
	Arrhenius constant *B*	17,595	17,595	17,595	17,595	17,595	17,595
	Weibull scale per flight hour for one stator module	1,282	1,282	1,282	1,282	1,282	1,282
	Weibull shape for stator module	3.0	3.0	3.0	3.0	3.0	3.0
	Cfactor – Stator thermal cycling factor	2.0	2.0	2.0	2.0	2.0	2.0
	Bearing reliability at motor scheduled retirement lifetime	0.9000	0.9000	0.9990	0.9995	0.9990	0.9990
	Bearing Weibull shape parameter	1.5	1.5	1.5	1.5	1.5	1.5
	Bearing HUMS[a] success rate, percentage as decimal	0.98	0.00	0.00	0.00	0.95	1.00
Outputs	Average failure rate without FT	6.62×10^{-5}	6.62×10^{-5}	4.00×10^{-5}	3.99×10^{-5}	4.00×10^{-5}	4.00×10^{-5}
	Average failure rate with FT	4.84×10^{-7}	2.38×10^{-5}	2.85×10^{-7}	1.72×10^{-7}	7.02×10^{-8}	5.89×10^{-8}
	Average failure rate ratio	137	3	140	232	570	680
	Mean time to failure ratio	106	2	120	199	488	582

[a]Health and usage monitoring system.

Results for run 5. The calculation for run 5 matched the inputs for run 3 except for the bearing HUMS success rates, which were 0.00 for run 3 and 0.95 for run 5. For the motor with FT stator, the introduction of a modestly successful bearing HUMS in combination with good bearing inherent reliability produced an overall average failure rate improvement ratio of about 570. This average failure rate ratio of 570 is a realistic estimate of the reliability improvement that could be achieved with the FT eVTOL modular concept motor.

Results for run 6. To complete this reliability study, run 6 was completed matching the inputs for run 5 except that the bearing HUMS success rate was 100%. This was done to determine the upper bound for the reliability improvement that could be achieved using the modular FT stator technology, because with a 100% successful HUMS, a bearing fault never results in a failed state. The average failure rate ratio was 680, and the mean time to failure the improvement ratio was 582. This value for *MTTF* ratio compares favorably with the 750 value determined by Jahns and Swanke (2024) using the time-homogeneous model approach (see Table V).

These results employing the time-inhomogeneous Markov-Weibull model further substantiate the study findings of Jahns and Swanke (2024) and their conclusion that FT modular motor drives are powerful architectures for reliable electric aircraft propulsor drives.

3.4 Motor Reliability Model Summary

Two reliability modeling tools for calculation of reliability of FT (and non-FT) motors were completed. The pair of models are complementary tools for the stakeholder and user community. Both models are based on Markov chain theory. The first of the two models is especially valuable when motor concepts are known to the concept-design level of detail. The second model requires some additional design detail (preliminary design detail) of the concept such that the thermal profile of motor coils can be estimated by simulation. The first model is a time-homogeneous Markov chain model. The second model is a time-inhomogeneous Markov-Weibull chain model. The reliability models' characteristics are summarized in Table VIII.

4.0 Validation of FT Operation by Hardware Demonstration

A low-power demonstrator machine was fabricated and tested to demonstrate the feasibility of FT operation of an eVTOL FT concept motor. The experimental results to be described validate the feasibility of the high reliability predicted by the modeling results completed herein. In general, the test data that will be discussed align extremely well with the simulated results presented in Jahns and Swanke (2024). Faulted module tests included terminal open- and short-circuit testing. Additionally, turn-to-turn faults were built into one of the machine phases, enabling the external application of turn-to-turn short-circuit faults. The electromagnetic isolation achieved with the demonstrator machine was evaluated statically by exciting the modules at high frequency with a stationary rotor, and measurements confirmed the low mutual electromagnetic coupling between the two modules. Following are some details of the machine, testing, and experiment demonstration results. Interested readers can find more detail in Swanke (2023) and Jahns and Swanke (2024).

4.1 Demonstrator Machine Description

The demonstrator machine that was designed and built is a two-module, double-layer, 12-slot/14-pole fractional-slot concentrated-wound stator with a V-shape interior permanent magnet rotor topology. The stator is modularized into two

TABLE VIII.—SUMMARY OF MOTOR RELIABILITY MODEL CHACTERISTICS

Characteristics	Model 1	Model 2
Motor design detail needed	Concept design	Preliminary design
Components modeled in this report	Motor and integrated power electronics	Motor
Markov model type	Time homogeneous	Time inhomogeneous
Model for the failure rate of components	Constant with time	Increases with time
Model for repair actions	Constant repair rate with time	Discrete repair event post-flight
Scheduled motor replacement life	Solutions are not influenced by a scheduled replacement life	Scheduled replacement life is an input parameter of reliability calculation
Solution method	Analytical	Numerical time marching
Output capability	Mean time to failure (*MTTF*) and FOMs based on *MTTF*	All measures of a system failure distribution are available, i.e., *MTTF*, *AFR,* distribution percentiles, and FOMs based on such

three-phase winding sets, allowing for the loss of a module without loss of torque operation. Machine phases are electromagnetically isolated from one another using a combination of stator flux barriers and modified stator tooth tips. The winding is directly cooled by flowing a low-electrical-conductivity coolant through tubes placed between coils. Doing so provides physical separation between coils and isolates coils from thermal interactions between phases. Both effects are desirable features for FT machines. Machine outer dimensions and a feature summary are given in Figure 23. The overall core stack length of the machine is 25.4 mm. The winding fabrication process introduced jumper wires into one of the machine phases, allowing for the external application of turn-to-turn faults. Specifically, strands from turns 27, 36, and 44 (of 47) are wound outside the coil. These turns were selected due to their ease of removal during the winding process. These jumper wires allowed for a range of faulted turn combinations to be tested. The demonstrator machine has been tested up to 3,000 rpm (speed limit of the test dyne) under healthy condition and 1,000 rpm under faulted conditions.

4.2 Machine Performance Validation

Jahns and Swanke (2024) provide a full reporting of measured machine parameters and performance. Measurements of machine parameters and health condition testing can be found in the referenced document. Herein we report the testing of operation after a fault, that is, validation of FT operation. The fault modes tested included terminal open circuit, thermal isolation after a fault, terminal short circuit, and internal short circuits between turns.

4.2.1 Terminal Open-Circuit Operation

The most benign type of fault is the terminal open-circuit fault. A demonstration of an open-circuit fault and associated response is shown in Figure 24. At $t < 0$, both modules are operating in a healthy state at 50% current load. A fault occurs (channel 4 signal dipping to zero) where module 2 is open circuited. Module 1 of the modular design immediately responds by increasing its current by a factor of 2 to make up for the lost module without any interruption in shaft torque or noticeable difference in torque ripple. The test results demonstrate the developed modular motor drive system is capable of FT operation during open-circuit transients.

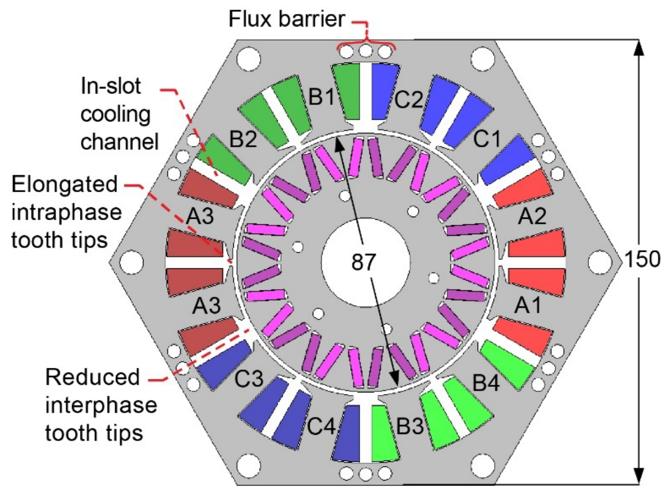

Figure 23.—Demonstrator isolation features, phase arrangement, and stator and rotor outer diameter dimensions in millimeters (Jahns and Swanke 2024).

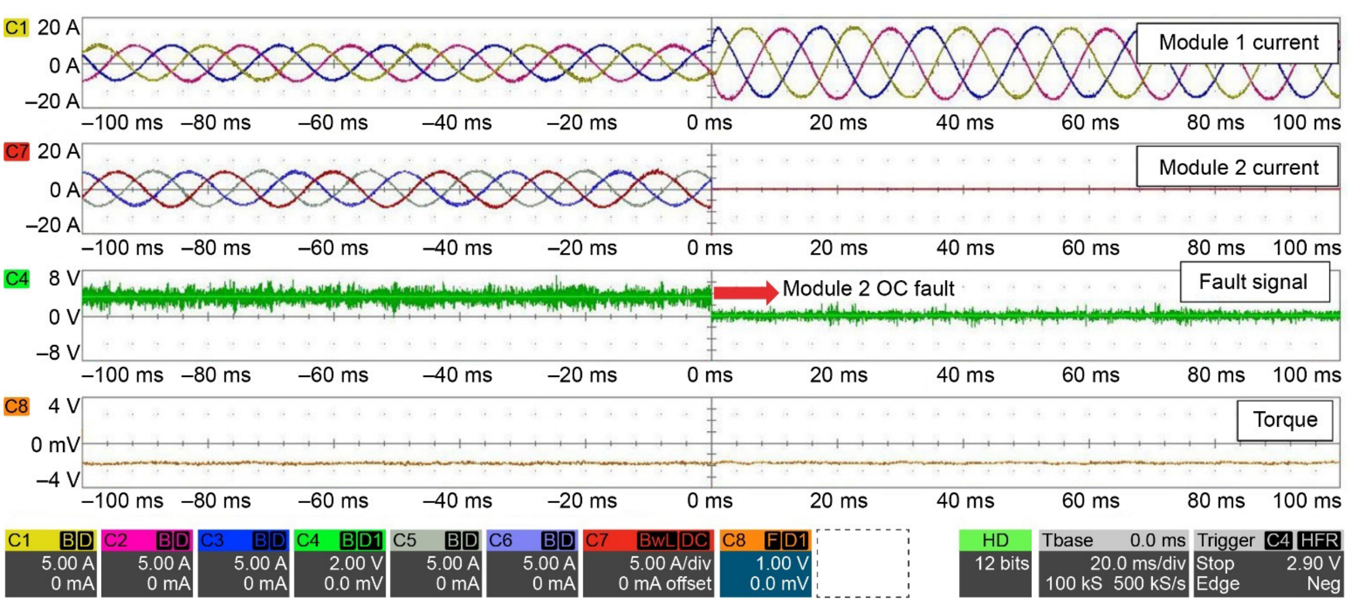

Figure 24.—Open-circuit fault demonstration at 500 rpm showing healthy operation, fault event, and postfault response (adapted from Swanke 2023).

4.2.2 Thermal Isolation After Fault

Thermal isolation between phases is a critical aspect of FT machine design. The developed design uses in-slot cooling channels to thermally buffer interactions between modules in the event of a failure. This is demonstrated under a full-current open-circuit test where module 2 is open circuit and module 1 delivers rated current—matching the postfault condition in Figure 24. Thermocouple transients are shown for this condition in Figure 25. The healthy module temperatures rise to expected levels observed under 100% current conditions (nearing 40 °C) while the open-circuit coils remain at lower temperatures near the coolant temperature. The observed sustained difference in temperature agrees with the thermal isolation simulation results in Jahns and Swanke (2024), verifying the essential FT thermal isolation feature of this FT design.

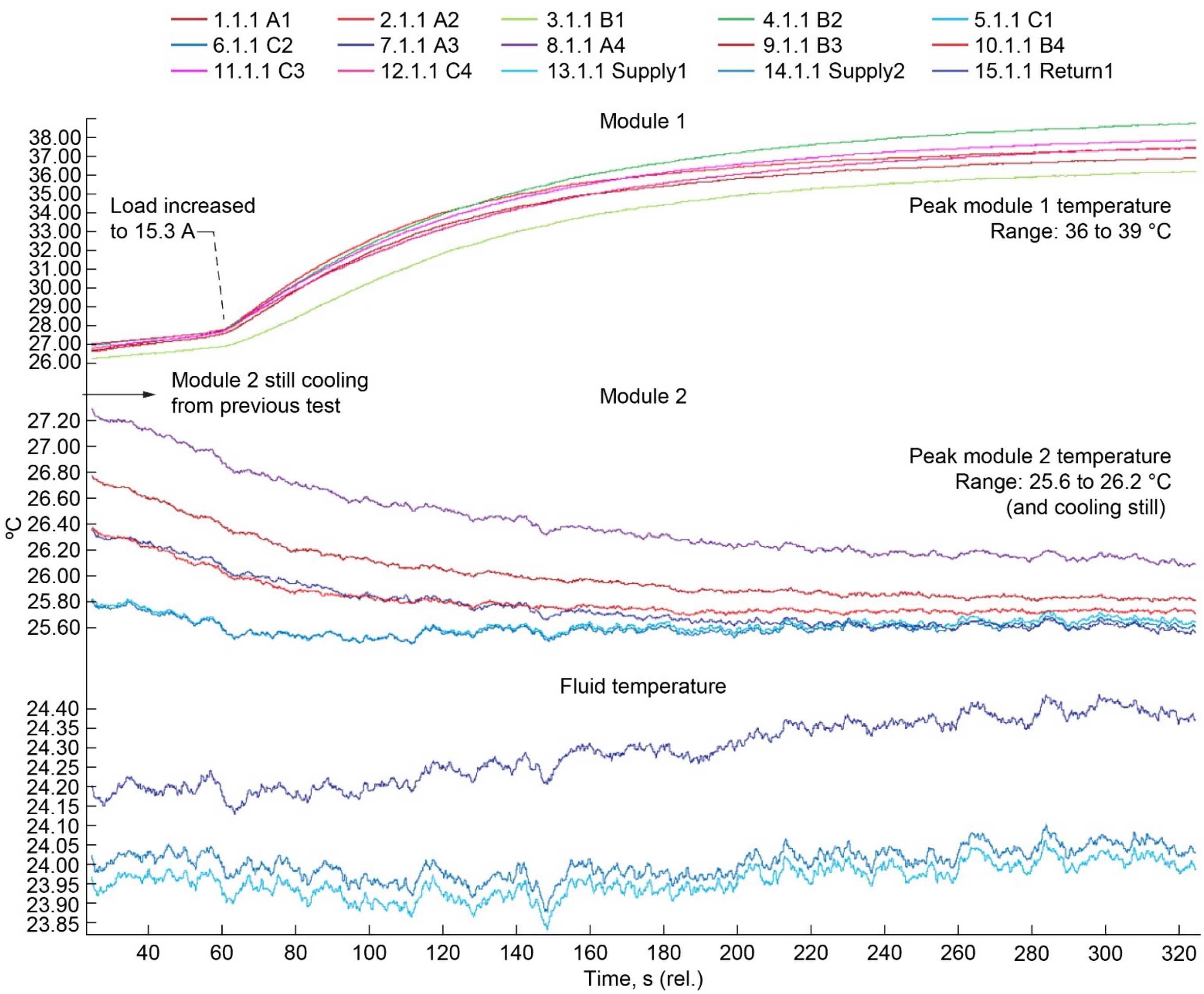

Figure 25.—Thermal isolation demonstration under full-load module 2 open-circuit fault (adapted from Swanke 2023).

4.2.3 Terminal Short-Circuit Operation

A more serious fault mode for permanent-magnet synchronous motors is high current transients from a terminal three-phase short circuit. Such postfault characteristic currents can potentially demagnetize rotor magnets. To mitigate such risks, the demonstrator motor was designed for high inductance (to minimize fault currents) and the magnet material was selected for strong coercivity at high temperatures to withstand peak transient currents at 3 times rated current. The short-circuit characteristics of the built machine were measured (Jahns and Swanke 2024), confirming characteristic current calculations of the design simulations. Demonstration of short-circuit operation follows a similar methodology similar to that of the previously discussed open-circuit case demonstration, that is, both modules operate under healthy conditions until, at $t = 0$, the terminal short-circuit fault is applied. The healthy module responds by increasing its current to compensate for the lost torque. The results of the test are shown in Figure 26. After the application of a three-phase short, a peak transient current of 15.3 A is observed. The data show that module 1's healthy currents are balanced and unaffected by adjacent faulted coils. The test results demonstrate successful FT operation during short-circuit transients.

4.2.4 Internal Short-Circuit Operation

The response of the motor after internal short-circuit faults was demonstrated. These faults can be especially harmful because of the significant current being driven through shorted turns by the rotor's permanent magnets. To study these faults, three-turn short circuits were brought out of a single phase in module 2, allowing for the external application of faults. Swanke and Jahns reported full results of passive testing of short-circuit faults ("passive" meaning that no current was delivered from the power electronics during testing), simulating the behavior after the fault is detected and the power electronics for the faulted module is disabled. During all passive testing, audible noise and vibration were observed for higher amplitude fault currents, highlighting some of the possible avenues for fault detection. The passive testing highlighted that fault currents develop rapidly in the event of an internal short circuit and can quickly become destructive. A passive turn-to-turn short thermal isolation test completed at 1,000 rpm corresponded to peak fault current of 33.5 A. Thermocouple measurements of the fault transient are shown in Figure 27. The faulted coil temperature rises dramatically in 2 min while only minor increases in temperature are observed in adjacent coils (~0.3 °C).

This experiment demonstrates the important role in-slot cooling has in FT machines for higher levels of fault current (e.g., single-turn faults at high speed): in-slot cooling provides sufficient thermal isolation on a transient basis to blunt the impact of elevated fault-related losses, giving time for the implemented fault detection scheme to identify the problem and react. Also, the response to an internal short circuit is demonstrated via an active test for a direct short between turns 44 and 47 at 500 rpm in Figure 28. Before $t = 0$, the machine is operating in an undetected fault state with a sustained internal short inside module 2 phase A. At $t = 0$, the fault is detected and a three-phase terminal short is applied to the windings, suppressing the faulted turn current. Healthy module 1 responds by increasing its phase current to compensate for the lost module 2 torque contributions.

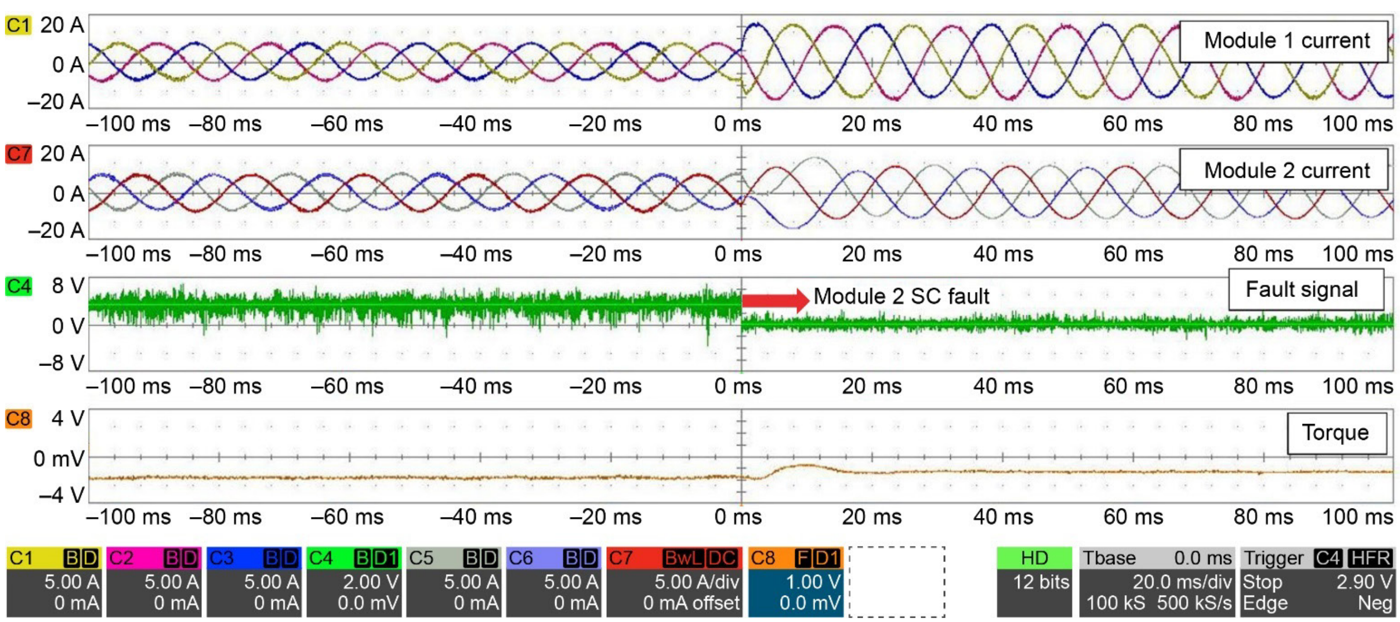

Figure 26.—Short-circuit fault demonstration at 500 rpm showing healthy operation, fault event, and postfault response (adapted from Jahns and Swanke 2024).

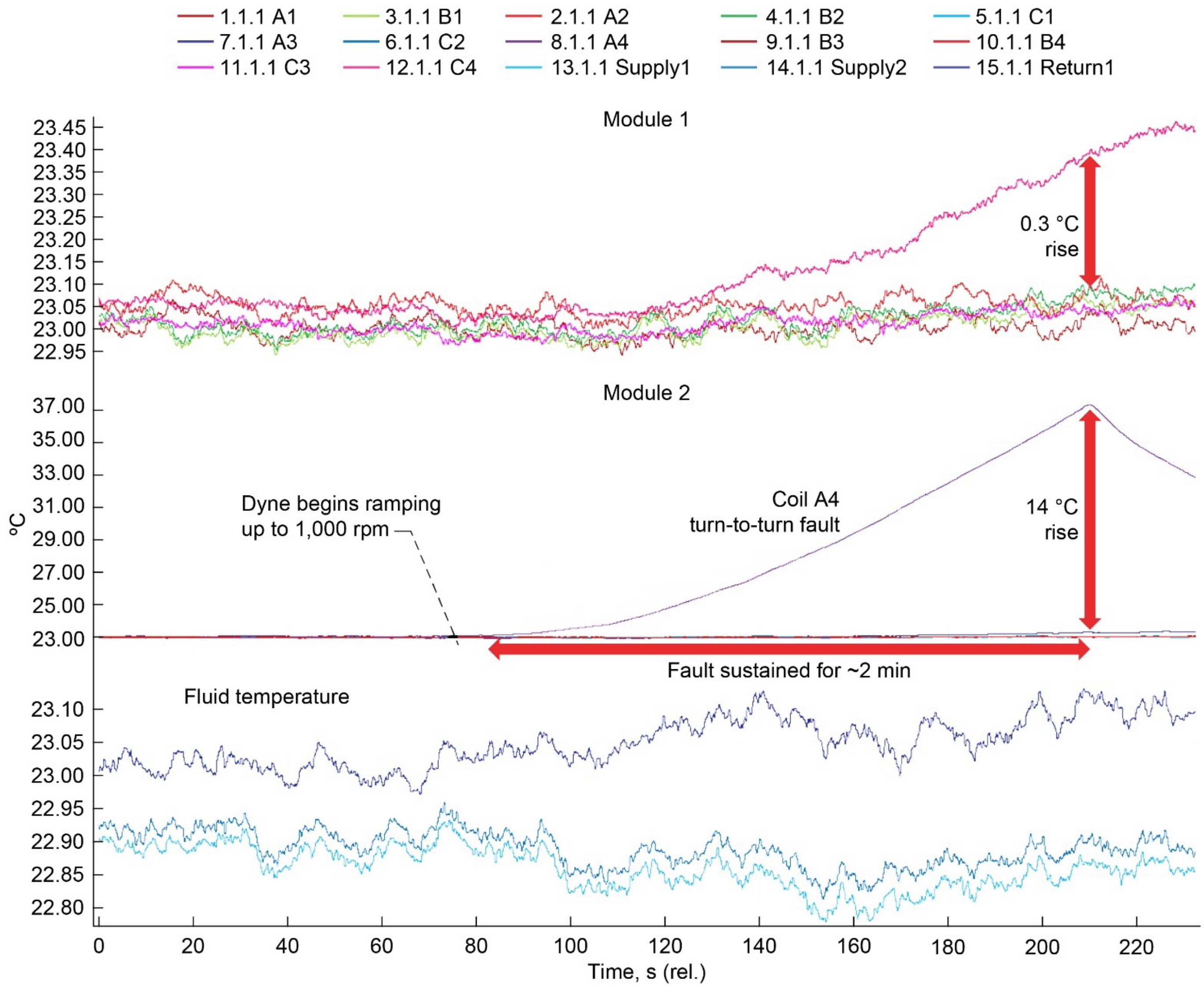

Figure 27.—Thermal transient during turn-to-turn fault between turns 27 and 44 (adapted from Swanke 2023).

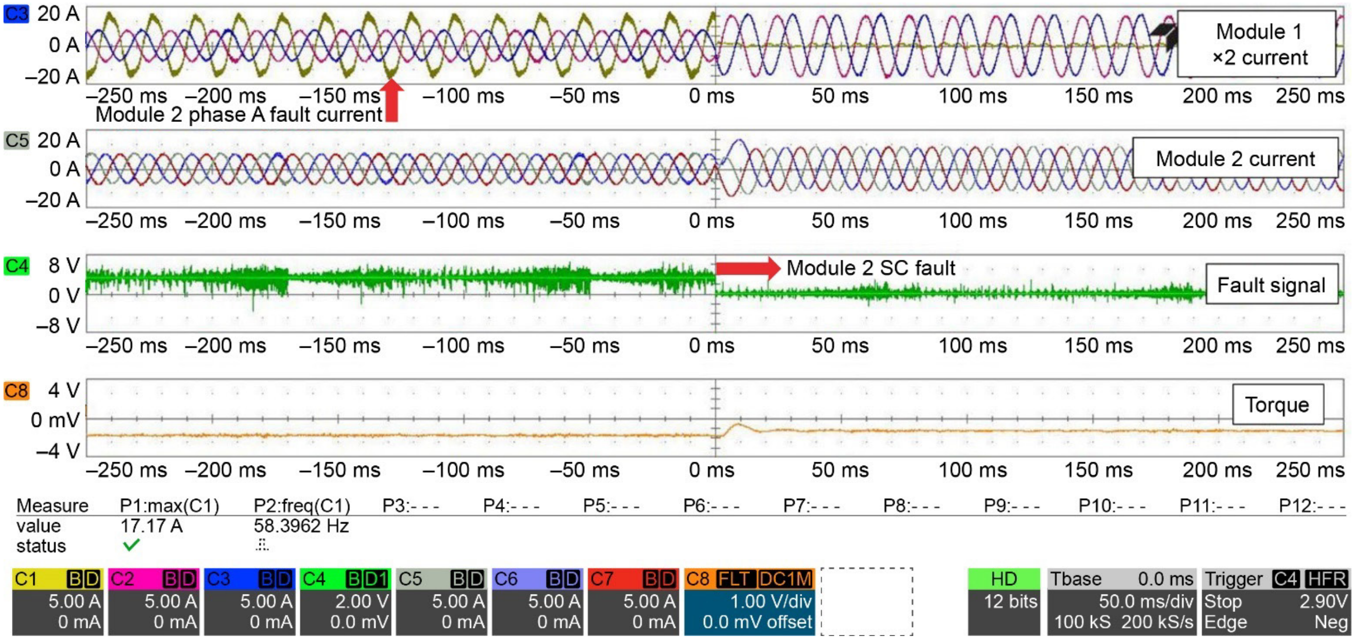

Figure 28.—Internal short-circuit fault demonstration at 500 rpm showing internal short-circuit current, fault response trigger, and postfault response (adapted from Jahns and Swanke 2024).

5.0 Concluding Remarks

This report documents research and results for NASA's Revolutionary Vertical Lift Technology Project and completes Project Annual Performance Indicator 24-3.2.4.1, "Apply and document reliability prediction for high-reliability motor concept." Motor reliability was defined for purposes of this study as the failure to produce demanded power during flight. Two reliability modeling tools for calculation of reliability of fault-tolerant (FT) (and non-FT) motors were completed. The pair of models are complementary tools for the stakeholder and user community. Both models are based on Markov chain theory. The first of the two models is especially valuable when motor concepts are known to the concept-design level of detail. The second model requires some additional design detail (preliminary design detail) of the concept such that the thermal profile of motor coils can be estimated by simulation. Model 1 is a time-homogeneous Markov chain model. Model 2 is a time-inhomogeneous Markov-Weibull chain model.

Six motor and drive concept designs were studied, and the relative reliabilities were compared using newly introduced fault tolerance figures of merit (FT-FOMs). The six designs of the study were (1) a baseline design without fault tolerance, (2) a five–phase machine drive with two allowable switch failures, (3) a direct redundant motor drive, (4) a two-module motor drive (X2-MMD), (5) a four-module motor drive (X4-MMD), and (6) and a four-module MMD with redundant resolver, redundant cooling system, and reduced-bearing SPF rates via a health monitoring system (X4-MMD+). Reliability model 1 was applied to these six concepts, and results were assessed. Using the mean-time-to-failure ratio as the measure of reliability improvement, the FT X4 MMD+ configuration was determined to be the most promising concept for eVTOL, having ~750 times greater reliability compared to the non-FT baseline standard configuration while also having favorable overrating factors and a modest mass penalty.

Given the results of the motor concepts case study, a four-module FT motor concept (X4-MMD+) was developed to preliminary-design level of detail. This eVTOL FT motor concept was designed for galvanic, magnetic, and thermal isolation of stator winding faults. The reliability of the concept motor was calculated using model 2. A reliability improvement of ~570 times greater reliability was achieved as compared to a baseline motor without fault tolerance. These results indicate that FT modular motor drives offer promise for addressing the daunting reliability gap that electric aircraft propulsor drives are facing relative to the best conventional motor drive technology that is available today.

To validate that these impressive modeling findings are feasible, the needed FT operation capabilities were demonstrated by experiment. The experimental test program has succeeded in demonstrating the key features of FT operation, providing experimental validation of the essential premises of the developed reliability models presented herein. The experiments included successful demonstration of the feasibility of the following four key FT features: (1) terminal open-circuit operation, (2) thermal isolation after fault, (3) terminal short-circuit operation, and (4) internal short-circuit operation.

Appendix A.—Nomenclature

A.1 Acronyms

CDF	cumulative distribution function
DC	direct current
eVTOL	electric vertical takeoff and landing
FOM	figure of merit
FS	failed state
FT	fault tolerant
FT-B	spalled bearing fault state
FT-FOM	fault tolerance figure of merit
FT-S	faulted modular winding state
HUMS	health and usage monitoring system
IMMD	integrated modular motor drive
MMD	modular motor drive
MMF	machine-mass (scaling) factor
MOSFET	metal-oxide-semiconductor field-effect transistor
MTMF	mean time to module group failure
MTTF	mean time to failure
MTTSPF	mean time to single point failure
NIST	National Institute of Standards and Technology
PDF	probability density function
PU	per unit
R-S	remove from service
RVLT	Revolutionary Vertical Lift Technology
SEMATECH	Semiconductor Manufacturing Technology
SPF	single-point failure
UMP	unbalanced magnetic pull
VDC	volts DC
VSI	voltage source inverter
X2-MMD	two-module motor drive
X4-MMD	four-module motor drive
X4-MMD+	X4-MMD with reduced SPF modes and rates

A.2 Symbols

A	constant dependent on geometry, size, fabrication methods, and other factors
A'	constant characteristic of chemical reaction
$\overline{A}$	faulted quadrant A
AFR	average failure rate
B	constant dependent on geometry, size, fabrication methods, and other factors
C	basic dynamic rating
D	cumulative damage fraction
DF	total damage fraction
DF_C	thermal cyclic damage
DF_T	thermal chemical damage
DMF	power electronics drive-mass scaling factor
E_a	activation energy
F	probability of failure
$F(t)$	cumulative distribution function
f_1, f_2	transition paths, unit 1 or 2 respectively
$f(t)$	probability density function
FS	failed state
$\boldsymbol{H}$	healthy state
$H(t)$	cumulative hazard function
$h(t)$	hazard function
I	electric current
i	discrete time instance
i_j	electrical current, phase j
k	Boltzmann's constant
Δkg	increase of mass relative to the non-fault-tolerant baseline
$KVAOF$	kilovolt-amp overrating factor
L_{10}	lifetime of the tenth percentile of the probability distribution in millions of revolutions
L_{50}	median lifetime
$\mathcal{L}$	Laplace transform to the s-domain
$\boldsymbol{M}$	faulted states
M_1, M_2	elements of faulted state vector $\boldsymbol{M}$
MMF	machine-mass scaling factor
$MTMF$	mean time to failure of the module group
$MTTF$	mean time to failure
$MTTF_{HR}$	mean time to failure for the topology using a high repair rate
$MTTF_{NR}$	mean time to failure with no repairs
$MTTF_{std}$	mean time to failure of a system without fault-tolerant operating capability

m_{em}	mass of the baseline motor
m_{pe}	mass of the baseline power electronics
N_{cycles}	number of cycles
$N_{r,s}$	number of cycles to failure for a given thermal range and peak
$\overline{N_i}$	mean lifetime for a constant temperature T_i
n_i	duration of the application of temperature T_i
OF	overrating factor
P	equivalent applied load
$\mathbf{P}$	Markov transition matrix, finite difference form
P_{jk}	one term of Markov transition matrix **P**
p	load-life exponent
Pr	probability
S	probability of survival
$S(t)$	survival function
T	temperature
$\mathbf{T}$	Markov transition matrix, differential equation form
T'	failure time
ΔT_r	range of thermal cycle
t	time; fatigue lifetime
t_1, t_2	time intervals
$Tpeak_s$	peak temperature
V	voltage
V'	stress level
V_C	DC link capacitor
V_{DC}	input voltage
$\boldsymbol{X}$	system state
$\dot{\boldsymbol{X}}$	derivative of $\boldsymbol{X}$ with respect to time t
β	shape parameter, Weibull distribution
γ	location parameter, Weibull distribution
η	scale parameter, Weibull distribution
λ_{m0}	module fault rate from the healthy state
λ_{m1}	additional module fault rate
λ_{s0}	single-point failure
λ_{BL}	baseline component failure rate
μ	repair rate
π_{brg}	pi-factor, bearing
π_{cap}	pi-factor, capacitor
π_{cls}	pi-factor, coils
π_i	pi-factor, multisource
π_{sw}	pi-factor, switch

References

Alarid-Escudero, Fernando, Eline Krijkamp, Eva A. Enns, Alan Yang, M.G. Myriam Hunink, Petros Pechlivanoglou, and Hawre Jalal. A Tutorial on Time-Dependent Cohort State-Transition Models in R Using a Cost-Effectiveness Analysis Example. Medical Decision Making 43, no. 1 (2023): 21-41. https://doi.org/10.1177/0272989x221121747

Baliga, B. Jayant. Power Semiconductor Device Figure of Merit for High-Frequency Applications. IEEE Electron Device Letters 10, no. 10 (1989): 455-457. https://doi.org/10.1109/55.43098

Beck, J. Robert, and Stephen G. Pauker. The Markov Process in Medical Prognosis. Medical Decision Making 3, no. 4 (1983): 419-458. https://doi.org/10.1177/0272989x8300300403

Boyd, Mark A., and Sonie Lau. An Introduction to Markov Modeling: Concepts and Uses. Annual Reliability and Maintainability Symposium 1998, Anaheim, California, January 19-22, 1998. NASA Document ID 20020050518. https://ntrs.nasa.gov

Chen, Yong, Siyuan Liang, Wanfu Li, Hong Liang, and Chengdong Wang. Faults and Diagnosis Methods of Permanent Magnet Synchronous Motors: A Review. Appl. Sci. 9, no. 10 (2019): 2116. https://doi.org/10.3390/app9102116

Dakin, Thomas W. Electrical Insulation Deterioration Treated as a Chemical Rate Phenomenon. Transactions AIEE 67, no. 1 (1948): 113-122. https://doi.org/10.1109/T-AIEE.1948.5059649

Darling, Richard W.R., and James R. Norris. Differential Equation Approximations for Markov Chains. Probability Surveys 5 (2008): 37-79.

Darmstadt, Patrick R., Ralph Catanese, Allan Beiderman, Fernando Dones, Ephraim Chen, Mihir P. Mistry, Brian Babie, Mary Beckman, and Robin Preator. Hazards Analysis and Failure Modes and Effects Criticality Analysis (FMECA) of Four Concept Vehicle Propulsion Systems. NASA/CR-2019-220217, 2019. https://ntrs.nasa.gov

Darmstadt, Patrick R., Sheevangi Pathak, Ephraim Chen, Mihir P. Mistry, Andrew Arkebauer, Allan Beiderman, Caitlin Dillard et al. Reliability and Safety Assessment of Urban Air Mobility Concept Vehicles. NASA CR-20210017188, 2021. https://ntrs.nasa.gov

Griffo, Antonio, Igor Tsyokhla, and Jiabin Wang. Lifetime of Machines Undergoing Thermal Cycling Stress. In 2019 IEEE Energy Conversion Congress and Exposition (ECCE), pp. 3831-3836. IEEE, 2019. https://doi.org/10.1109/ECCE.2019.8913216

Harris, Tedric A. Rolling Bearing Analysis, 2nd edition. John Wiley & Sons, 1984.

House, Thomas. Lie Algebra Solution of Population Models Based on Time-Inhomogeneous Markov Chains. J. App. Prob. 49, no. 2 (2012): 472-481. https://doi.org/10.1239/jap/1339878799

Iskandar, Rowan. A Theoretical Foundation for State-Transition Cohort Models in Health Decision Analysis. PloS One 13, no. 12 (2018). https://doi.org/10.1371/journal.pone.0205543

Jackson, Alazel. Reliability Modeling That Combines Markov Analysis and Weibull Distributions. In 2013 Proceedings Annual Reliability and Maintainability Symposium (RAMS), pp. 1-6. IEEE, 2013. https://doi.org/10.1109/RAMS.2013.6517742

Jahns, Thomas M., and James A. Swanke III. Extended Investigation into Fault-Tolerant Integrated Motor Drive for a Quadrotor Urban Air Mobility (UAM) Aircraft. NASA CR-20240005899, 2024. https://ntrs.nasa.gov

Johnson, Barry. Fault-Tolerant Microprocessor-Based Systems. IEEE Micro 4, no. 6 (1984): 6-21. https://doi.org/10.1109/MM.1984.291277

Lipo, Thomas A. Introduction to AC Machine Design. John Wiley & Sons, 2017.

Madonna, Vincenzo, Paolo Giangrande, Giovanni Migliazza, Giampaolo Buticchi, and Michael Galea. A Time-Saving Approach for the Thermal Lifetime Evaluation of Low-Voltage Electrical Machines. IEEE Transactions on Industrial Electronics 67, no. 11 (2019): 9195-9205. https://doi.org/10.1109/TIE.2019.2956378

Markov, A.A. The Extension of the Law of Large Numbers onto Quantities Depending on Each Other. In Probability and Statistics Russian Papers, selected and translated by Oscar Sheynin. NG Verlag, 2004.

Meeker, William Q., and Luis A. Escobar. Statistical Methods for Reliability Data. John Wiley & Sons, 1998.

MIL-HDBK-217F, Military Handbook: Reliability Prediction of Electronic Equipment. 1991.

Miner, Milton A. Cumulative Damage in Fatigue. J. Appl. Mech. 12(3) (1945): A159-A164. https://doi.org/10.1115/1.4009458

NASA-STD-5017B, Design and Development Requirements for Mechanisms. NASA Technical Standards System. https://standards.nasa.gov/standard/NASA/NASA-STD-5017

National Aeronautics and Space Administration. NASA Aeronautics Strategic Implementation Plan 2023. NASA Aeronautics Research Mission Directorate. https://www.nasa.gov/directorates/armd/armd-strategic-implementation-plan/, accessed 6/4/2024.

Nelson, Wayne B. Accelerated Testing: Statistical Models, Test Plans, and Data Analysis. John Wiley & Sons, 1990.

NIST/SEMATECH e-Handbook of Statistical Methods. National Institute of Standards and Technology. https://doi.org/10.18434/M32189

Palmgren, Arvid. Ball and Roller Bearing Engineering, 3rd ed. Translation by Gunnar Palmgren and Bryce Ruley. SKF Industries Inc., 1959.

Rausand, Marvin, and Arnljot Hoyland. System Reliability Theory: Models, Statistical Methods, and Applications. Vol. 396. John Wiley & Sons, 2003.

Shah, D., N. Khan, N. Hawkins, and A. Briggs. PRM14 Time-Dependency for Treatment Sequences in Markov Cohort Models: A Nested Markov Modeling Approach. Value in Health 15, no. 4 (2012): A161.

Shimokawa, Toshiyuki, and Sakae Tanaka. A Statistical Consideration of Miner's Rule. Int. J. Fatigue 2, no. 4 (1980): 165-170. https://doi.org/10.1016/0142-1123(80)90044-4

Silva, Christopher, Wayne R. Johnson, Eduardo Solis, Michael D. Patterson, and Kevin R. Antcliff. VTOL Urban Air Mobility Concept Vehicles for Technology Development. In 2018 Aviation Technology, Integration, and Operations Conference, p. 3847. 2018. https://doi.org/10.2514/6.2018-3847

Sjökvist, Stefan. Demagnetization Studies on Permanent Magnets: Comparing FEM Simulations With Experiments. Ph.D. Dissertation, Acta Universitatis Upsaliensis, 2014.

Smith, Robert J., and Alastair R. Flew. Redundancy for Electric Motors in Spacecraft Applications. In 20th Aerospace Mechanisms Symposium, Conference Proceedings, NASA-CP-2423, 1986. https://ntrs.nasa.gov

Sonnenberg, Frank A., and J. Robert Beck. Markov Models in Medical Decision Making: A Practical Guide. Medical Decision Making 13, no. 4 (1993): 322-338. https://doi.org/10.1177/0272989x9301300409

Sung, Woongje, Kijeong Han, and B. J. Baliga. Optimization of the JFET Region of 1.2 kV SiC MOSFETs for Improved High Frequency Figure of Merit (HF-FOM). In 2017 IEEE 5th Workshop on Wide Bandgap Power Devices and Applications (WiPDA), pp. 238-241. IEEE, 2017. https://doi.org/10.1109/WiPDA.2017.8170553

Swanke, James A., III. Fault-Tolerant Integrated Modular Motor Drive for Applications With Demanding Reliability Requirements. Ph.D. Dissertation, Univ. of Wisconsin-Madison, 2023.

s

Swanke, James, Hao Zeng, and Thomas M. Jahns. Modular Fault-Tolerant Machine Design With Improved Electromagnetic Isolation for Urban Air Mobility (UAM)Aircraft. In 2021 IEEE Energy Conversion Congress and Exposition (ECCE), pp. 4570-4577. IEEE, 2021. https://doi.org/10.1109/ECCE47101.2021.9595489

Swanke, James A., and Thomas M. Jahns. Reliability Analysis of a fault-Tolerant Integrated Modular Motor Drive for an Urban Air Mobility Aircraft Using Markov Chains. IEEE Transactions on Transportation Electrification 8, no. 4 (2022): 4523-4533. https://doi.org/10.1109/TTE.2022.3183933

Swanke, James A., Hao Zeng, Thomas M. Jahns, and Bulent Sarlioglu. Systematic Motor Drive Reliability Improvement Methodology Using Fault-Tolerant Modular Motor Drives. In 2023 IEEE Energy Conversion Congress and Exposition (ECCE), pp. 1794-1801. IEEE, 2023. https://doi.org/10.1109/ECCE53617.2023.10362384

Tallerico, Thomas Francis, Andrew Douglas Smith, and Jeffryes Walter Chapman. Design Optimization Study of Fault-Tolerant and Redundant Motor Drivetrains for Urban Air Mobility Vehicles. In 2023 IEEE International Electric Machines and Drives Conference (IEMDC), pp. 1-5. IEEE, 2023. https://ntrs.nasa.gov

Wang, Yingnan, Chengming Zhang, Chaoyu Zhang, and Liyi Li. Review of High-Power-Density and Fault-Tolerant Design of Propulsion Motors for Electric Aircraft. Energies 16, no. 19 (2023): 7015.

Weibull, Waloddi. The Phenomenon of Rupture in Solids. IVA Handlingar 153 (1939).

Weibull, Waloddi. A Statistical Distribution Function of Wide Applicability. J. App. Mech. 18, vol. 3 (1951). https://doi.org/10.1115/1.4010337

Welchko, Brian A., Thomas A. Lipo, Thomas M. Jahns, and Steven E. Schulz. Fault-Tolerant Three-Phase AC Motor Drive Topologies: A Comparison of Features, Cost, and Limitations. IEEE Transactions on Power Electronics 19, no. 4 (2004): 1108-1116. https://doi.org/10.1109/TPEL.2004.830074